Development of a Fiber-Optical Probe for Near-Infrared Raman Spectroscopy in Tissue

Master's Thesis
by
Sara Pålsson

Lund Reports on Atomic Physics, LRAP-221
Lund, September 1997

This thesis was submitted to the
Faculty of Technology at Lund University
in partial fulfilment of the requirements for
the degree of Master of Science.

Abstract

A fiber-optical probe for near-infrared Raman spectroscopy in tissue was developed and evaluated. The probe allows remote Raman spectroscopy measurements by guiding the excitation light and scattered light through fibers. The probe eliminates the fiber emission of the guiding fibers by band pass filtering of the excitation light and long pass filtering of the scattered light. Only, the fiber emission from a short measuring fiber for *in vivo* measurements remains. Four different fiber makes were tested with respect to the fiber emission amount and transmission and it was found that the Anhydroguide fiber (AFS400/440B, Fiberguide Industries, Inc) was the most suitable choice for near-infrared Raman spectroscopy. Further, two probe configurations were tested and the one with a holographic beamsplitter that reflects the excitation light into the measuring fiber proved to be the most appropriate. The final probe is small, stable, easy to align and has a perfect performance.

Table of contents

1. Introduction

This thesis deals with the development of a fiber optical probe for near-infrared Raman spectroscopy. Raman spectroscopy is one of many optical spectroscopy techniques that can be used to study physical and biochemical changes in tissue. Laser-induced fluorescence is extensively used for clinical diagnosis of tissue, but there are also other optical spectroscopic techniques that are potential candidates for tissue diagnosis, e.g. Raman spectroscopy, IR absorption spectroscopy and diffuse reflectance measurements.

Presently, most diagnoses are based on visual examination of x-ray images, ultrasonography images or magnetic resonance images in order to localize potentially diseased areas. However, many diseases, e.g. cancers, do not show any physical change until the disease is fully developed and thus lethal. Early detection and treatment are the major goals in modern medicine and it may be accomplished by optical spectroscopy that probes the early biochemical changes in diseased tissue.

Normally, whenever there is a suspected disease, biopsies are taken and examined in the laboratory. The histological examination gives reliable and detailed information of the tissue sample but the method has some drawbacks. The removal of tissue is a surgical operation and there is always the possibility of taking the sample at the only healthy spot in a diseased environment. In addition, there is a time delay between tissue removal and examination.

Raman spectroscopy probes the vibration modes of the molecules in a sample and gives narrow peaks which correspond to specific vibration frequencies. Fluorescence spectroscopy gives broad emission bands originating from a limited number of biological molecules. In contrast to fluorescence, almost all molecules are Raman active. These reasons indicate that Raman spectroscopy could be a better method for tissue classification. However, Raman scattered light is very weak and it is hidden in the tissue fluorescence. One therefore has to use methods to reduce fluorescence and enhance Raman scattered light. One way is to use near-infrared excitation light which has an energy low enough to reduce fluorescence from most molecules.

In the past, most tissue spectroscopy was done *in vitro*. However, removal and handling of the tissue sample may cause artefacts in the diagnosis and there is the same time delay between sample taking and examination as with all biopsies. The development of fiber optics allows tissue spectroscopy to be done non-intrusively *in vivo*. The light is guided by a fiber which can be led through a normal endoscope, injected with a needle or placed in the blood vessels. In this way, spectroscopy can be used for on-line direct diagnosis and/or guiding the collection of biopsies to suspected areas. This has been done with laser induced fluorescence and there are commercial systems available. Another advantage with fibers is that the laser, spectrograph and detector do not have to be close to the measuring place. In clinical use, the equipment could be placed in a corner of an operating room and the light could be guided with fibers to the patient. Unfortunately, fibers have one big drawback in conjunction with Raman spectroscopy, namely the emission of the fibers themselves. Fibers are made of silica which always contains some impurities that cause both fiber fluorescence and Raman peaks. This project deals with the development of a probe which, by filtering away some fiber emission, allows long fiber lengths for remote Raman spectroscopy. The probe should be small and easy to align and handle.

The project is a part of the continuous research at Lund University Medical Laser Centre to develop methods to use near-infrared Raman spectroscopy for tissue characterisation, see Refs. [1-4].

In chapter 2 there is a brief summary of the different scattering processes that cause Raman scattering and fluorescence and in chapter 3 there is a survey of equipment for Raman spectroscopy in tissue, methods to reduce tissue fluorescence and a short introduction to Raman diagnostics in tissue. The basic concepts of fibers and the origin and ways to remove fiber emission background are discussed in chapter 4. In chapter 5, the measurements for the determination of the best make of fiber are presented and in chapter 6, two different probe configurations are described, tested and evaluated. The final probe is tested and evaluated in chapter 7 and in chapter 8, there is a summary of the project. The appendix includes all drawings of the probe.

2. Theory of Raman Scattering

2.1 Introduction

Whenever light passes through a medium, some of it will be absorbed by molecules in the medium and some of it will be scattered. Raman scattering is an inelastic scattering process that may be used to probe the rotation and vibration energies of molecules. This chapter gives a brief survey of different scattering processes in general and Raman scattering in particular.

2.2 Scattering Processes

Scattering can be elastic or inelastic. It is said to be elastic when there is no net energy transfer between light and medium, and inelastic when energy is given or taken from the medium. After inelastic scattering, the scattered light has a different wavelength than the incoming light.

2.2.1 Elastic Scattering

There are two kinds of elastic scattering, Rayleigh and Mie scattering. When the size of a scattering particle is considerably larger than the wavelength, the light will be Mie scattered. The probability of Mie scattering is a very complex function of wavelength, the geometry of the particle, the refraction indices of the particle and the surrounding media, and the probability for absorption. In general, the intensity of the scattered light increases with shorter wavelengths and follows approximately a λ^{-2} dependence.

Rayleigh scattering occurs when light interacts with molecules smaller than the wavelength. The varying electric field creates a polarisation in molecules which act like antennas and reemit the light in a new direction. There can be both resonant and non-resonant Rayleigh scattering. The resonant Rayleigh scattering occurs when the energy of the light corresponds to the energy of an electronic state in the molecule. The probability for Rayleigh scattering increases with shorter wavelengths and follows a λ^{-4} dependence. The wavelength dependence of Rayleigh and Mie scattering is the cause of the blue sky and the red sunset. A summary of scattering processes (except Mie scattering) can be found in Figure 2-1.

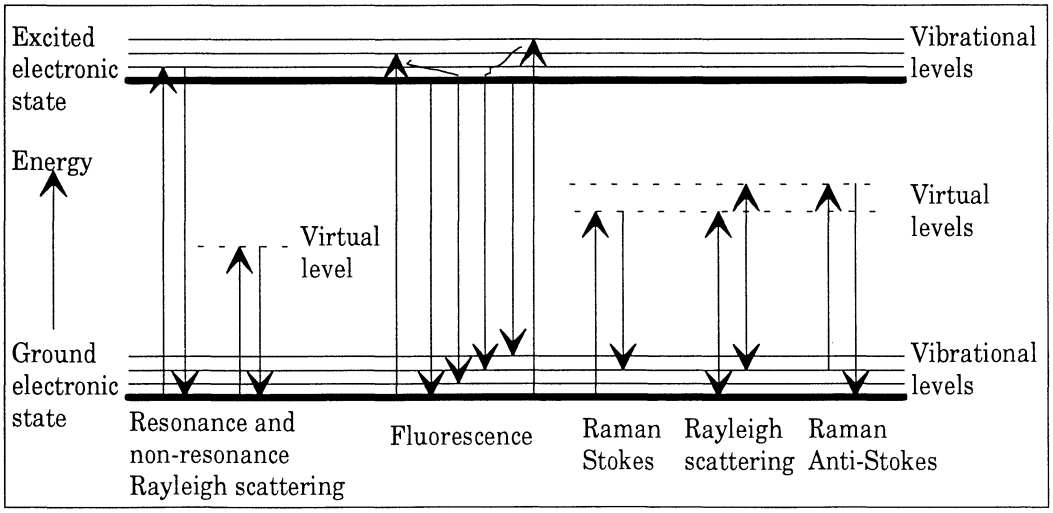

Figure 2-1 Different scattering processes.

2.2.2 Inelastic Scattering

In addition to electronic states, molecules have rotational and vibrational energy states. Incoming light can interact with these states. The scattering is inelastic if the scattered light has another wavelength than the incoming light. If the energy of the incoming light is high enough to excite the molecule to a higher electronic state, the molecule may absorb the light. After a very short time, the molecule relaxes with a non-radiative process to the lowest level in the excited state by so called internal conversion. This relaxation is caused by collisions with other molecules. Like everything else in the nature, the molecule strive to be in the lowest possible energy state. From the excited state, the molecule can give away its energy in different ways. The energy can be transferred to a triplet state in the molecule or it can be transferred to an other molecule in the vicinity. The molecule can also emit fluorescence light or get deexcited by collisions. After the relaxation, the molecule ends up in one of the vibrational levels in the ground state.

If the energy of the incoming light is too small to excite the molecule to the lowest electronic state, then Rayleigh or Raman scattering may take place. The molecule is excited to a non-existing virtual level and from there light may be emitted. Depending on if energy is preserved, lost or gained, we talk about Rayleigh scattering, Stokes or Anti-Stokes Raman scattering, respectively, see Figure 2-1.

2.3 Raman Theory

This chapter gives an introduction to the origin of Raman spectra and the theories that can be applied to describe the Raman phenomenon. A classical model with an oscillating electronic dipole and a mathematically more correct quantum-mechanical model are considered.

2.3.1 Vibration and Rotation Energies in Molecules

When two or more atoms form a molecule there will be additional rotation and vibration energies besides the electronic states. A vibration mode is a movement that does not move the centre of gravity and rotation is rotation around a principal axis in the molecule.

The vibrational modes can be divided into two different groups: Stretching modes, where the distance between the atoms or groups of atoms are altered and bending modes, where the angle between atoms or groups of atoms are altered. Some examples of vibrational modes are found in Figure 2-2.

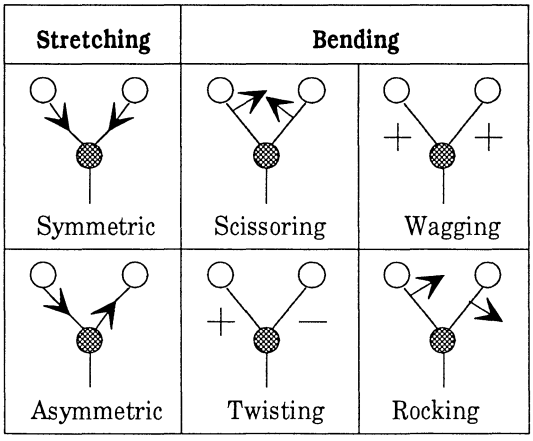

Figure 2-2 Vibrational modes for atoms or groups of atoms. The + and - signs indicate movement out of and into the plane of this page. Modified from Ref. [5].

Every atom has 3 degrees of freedom (the three coordinates to specify it's position in space) and thus a N-atomic molecule has 3N degrees of freedom. Three of these are rotational modes and three are translation modes. The rest 3N-6 modes are vibrational modes. If the molecule is linear (the atoms are placed along a straight line, for example CO_2 and N_2), then there will be 3N-5 vibrational modes since there can be only two independent rotational modes. Rotation around the axis does not count since it does not involve any movement of the nuclei.

The potential energy of a diatomic molecule at low energies can be approximated as a parabola. The molecule can then be treated as a harmonic oscillator and the classical vibration frequency ν_c is given by

$$\nu_c = \frac{1}{2\pi}\sqrt{\frac{k}{\mu}} \tag{2.1}$$

where μ is the reduced mass and k is the force constant. Quantum-mechanics gives the vibration energies

$$E_v = (v + \tfrac{1}{2})h\nu_c \quad v = 0, 1, 2, \ldots \tag{2.2}$$

This gives equidistant vibration levels with a non-zero lowest energy. The energy distance between two levels is typically 0.1 eV (1 eV = $1.602 \cdot 10^{-19}$ J). Remember that this calculation is only valid for diatomic molecules and low vibration energies. For the vibration modes in polyatomic molecules, the theory is much more complex.

The rotation energies are much smaller than the vibration energies, approximately 10^{-3} eV. The total energy of a molecule is given by the sum of it's vibrational, rotational and electronic energies. In Figure 2-3, there is a schematic model of the energy states in a molecule.

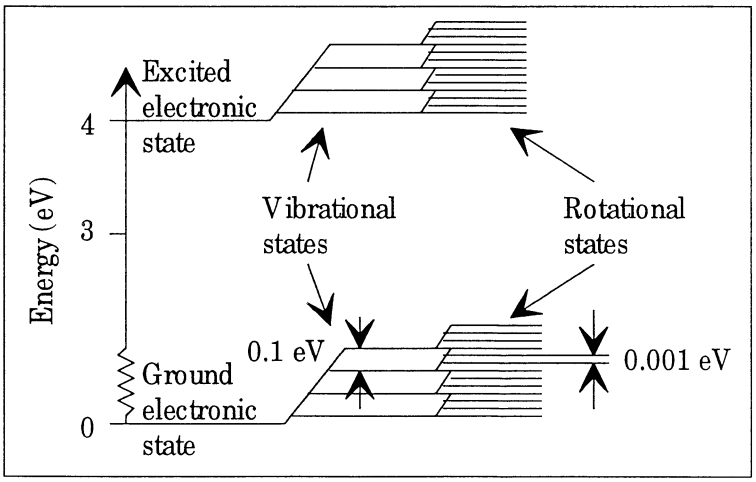

Figure 2-3 Energy states in a molecule. Modified from Ref. [5].

2.3.2 Classical Approach to Raman Theory

In the classical model, the molecule is approximated by a positively charged heavy nucleus with a negatively charged electron cloud around. In general, molecules are very small, ~1 nm, and thus the electrical field from incoming light with a wavelength in the visible region, λ = ~500 nm, would be the same throughout the molecule. The force acting on the individual electrons is the same and the electron displacements will be the same for all electrons. The displacements create an induced polarisation that will follow the electrical field.

The incident light can be described as an oscillating electric field E (the magnetic part of the electromagnetic wave does not contribute to any scattering phenomena).

$$E = E_0 \cos(2\pi \nu_0 t) \tag{2.3}$$

E_0 is the amplitude of the electric field, ν_0 the frequency of the oscillating electric field and t stands for time. This electric field acts like a force and displaces the electrons and creates a polarisation P.

$$P = \alpha E \tag{2.4}$$

α is the polarisability of the molecule and it describes how easy it is to manipulate its electrons and create an induced dipole. Normally, the polarisabilty α is not a scalar but a tensor since most molecules are asymmetric and hence the direction of the induced polarisation is not parallel to the direction of the initiating electrical field. The polarisation can be rewritten in Cartesian coordinates as a matrix equation.

$$\begin{bmatrix} P_x \\ P_y \\ P_z \end{bmatrix} = \begin{bmatrix} \alpha_{xx} & \alpha_{xy} & \alpha_{xz} \\ \alpha_{yx} & \alpha_{yy} & \alpha_{yz} \\ \alpha_{zx} & \alpha_{zy} & \alpha_{zz} \end{bmatrix} \begin{bmatrix} E_x \\ E_y \\ E_z \end{bmatrix} \tag{2.5}$$

Since the molecule vibrates, the displacement q from the equilibrium state can be written as

$$q = q_0 \cos(2\pi \nu_{vib} t) \tag{2.6}$$

where q_0 is the maximal displacement and ν_{vib} is the vibrational frequency. This displacement alters the polarisability of the molecule and for small displacements, the polarisability can be expanded in a Taylor series around the equilibrium state.

$$\alpha(q) = \alpha_0 + \left.\frac{\partial \alpha}{\partial q}\right|_{q_0} \cdot q + \text{(higher order terms)} \tag{2.7}$$

Inserting (2.3), (2.6) and (2.7) in (2.4) yields

$$P = \alpha_0 E_0 \cos(2\pi\nu_0 t) + \left.\frac{\partial\alpha}{\partial q}\right|_{q_0} \cdot q_0 E_0 \cos(2\pi\nu_{vib} t)\cos(2\pi\nu_0 t) \tag{2.8}$$

Using the trigonometric identity $\cos(\alpha)\cos(\beta) = \frac{1}{2}[\cos(\alpha+\beta)+\cos(\alpha-\beta)]$, this can be rewritten as

$$P = \alpha_0 E_0 \cos(2\pi\nu_0 t) + \frac{1}{2}\left.\frac{\partial\alpha}{\partial q}\right|_{q_0} \cdot q_0 E_0 [\cos(2\pi(\nu_0+\nu_{vib})t) + \cos(2\pi(\nu_0-\nu_{vib})t] \tag{2.9}$$

This polarisation is the driving term in the wave equation

$$\nabla^2\mathbf{E} - \frac{n^2}{c^2}\frac{\partial^2\mathbf{E}}{\partial t^2} = \mu_0 \frac{\partial^2\mathbf{P}}{\partial t^2} \tag{2.10}$$

which describes the emitted radiation from the oscillating dipole. The first term in (2.9) oscillates at ν_0 and describes the Rayleigh scattering and the second and third terms describe the Raman-scattered light with two components called Stokes (ν_0-ν_{vib}) and Anti-Stokes (ν_0+ν_{vib}). There will only be any Raman scattering on condition that $\left.\frac{\partial\alpha}{\partial q}\right|_{q_0} \neq 0$, which means that the polarisability must change when the displacement changes. Different molecules have different values on the derivative and are hence differently strong Raman scatterers.

The intensity from an oscillating dipole is given by

$$I = \frac{2}{3c^2}\overline{\left(\frac{\partial^2 P}{\partial t^2}\right)} \tag{2.11}$$

Inserting (2.9) in (2.11) yields

$$I_{Rayleigh} = C_R \alpha_0^4 \nu_0^4 I_0 \tag{2.12}$$

$$I_{Stokes} = C\left(\left.\frac{\partial\alpha}{\partial q}\right|_{q_0}\right)^2 (\nu_0 - \nu_{vib})^4 I_0 \tag{2.13}$$

$$I_{Anti-Stokes} = C\left(\left.\frac{\partial\alpha}{\partial q}\right|_{q_0}\right)^2 (\nu_0 + \nu_{vib})^4 I_0 \tag{2.14}$$

where C and C_R are constants and I_0 is the incident intensity. In (2.13) and (2.14) the intensity is proportional to the fourth power of the scattering frequency which means that the Raman scattered light strongly decreases when the wavelength is increased. The relative intensity of the Stokes and Anti-Stokes light would according to (2.13) and (2.14) be proportional to $[(\nu_0-\nu_{vib})/(\nu_0+\nu_{vib})]^4$. This is not in accordance with measured intensities where the Anti-Stokes component is much weaker than the Stokes component. To get the correct relative intensity dependence one has to consider the Raman scattering in a quantum-mechanical way.

2.3.3 Quantum-Mechanical Approach to Raman Theory

In the quantum-mechanical approach to Raman scattering, the vibration energies which give energy levels, see Figure 2-4, are taken into account.

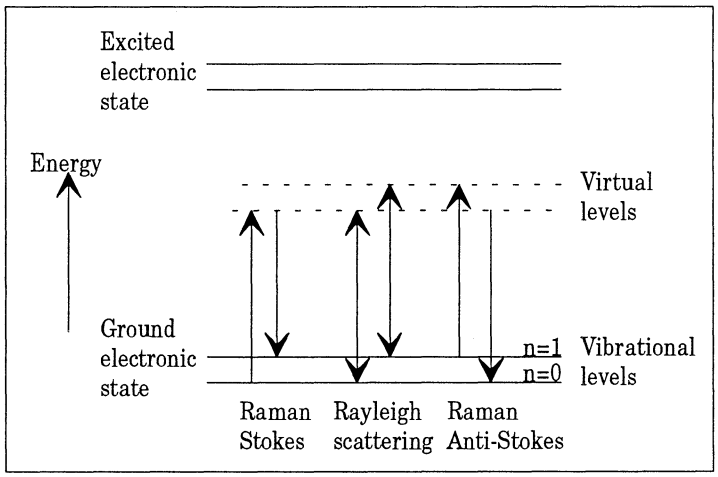

Figure 2-4 Raman scattering.

If the energy of an incident photon corresponds to the energy difference between two electronic states, the molecule can absorb the energy and change electronic state. However, in normal Raman scattering processes, the photon energy is too low to bring about an excitation to an electronic state. The incident photon just perturbs the molecular system for a very short moment. One says that the incident photon excites the molecule to a virtual level, and after a short while this energy is reemitted again, see Figure 2-4. A virtual level is forbidden according to quantum mechanics since it does not correspond to any possible vibrational, rotational or electronic mode.

An electronic level is divided into several vibration levels. If the molecule ends up with a higher vibration energy state than it had before the perturbation, the molecule has gained energy and the emitted light has been Stokes shifted by the same amount of energy as the energy difference between the vibrational modes. If the molecule loses energy, the reemitted light is said to be Anti-Stokes shifted.

At normal temperatures, almost all molecules are in their lowest vibrational state. The relation between the populations in two levels separated by ΔE is given by the Boltzmann law

$$\frac{N_{upper}}{N_{lower}} = e^{\frac{\Delta E}{kT}} \tag{2.15}$$

where N stands for the number of molecules per unit of volume in the upper and lower levels, respectively, k is the Boltzmann constant and T is the temperature. In order to get Anti-Stokes Raman scattering, the molecule has to be in an upper vibration level, $v \geq 1$. Since there are very few molecules in upper levels, the Anti-Stokes scattering is very weak. At room temperature (300 K) and for a vibrational energy of 0.1 eV, the ratio according to Boltzmanns law yields $N_{upper}/N_{lower} = 48$. The expression for the relative intensity between Stokes and Anti-Stokes Raman scattering, see equations (2.13) and (2.14), has to be modified with the Boltzmann law yielding

$$\frac{I_{Stokes}}{I_{Anti-Stokes}} = \frac{(\nu_0 - \nu_{ib})^4}{(\nu_0 + \nu_{ib})^4} e^{\frac{\Delta E}{kT}} \tag{2.16}$$

This relation is in agreement with experimental results. The Anti-Stokes is so weak that it is normally not used for practical spectroscopy. However, Coherent Anti-Stokes Raman Spectroscopy (CARS), see Ref. [5], is a frequently used technique for spectroscopy of flames and internal combustion engines. The Anti-Stokes component is obtained by a non-linear four-wave mixing between the excitation radiation and the generated Stokes components.

3. Raman Spectroscopy in Tissue

3.1 Introduction

The early attempts to measure Raman spectra of cells and tissues were hindered by the facts that there was no way to suppress fluorescence and that the instruments used had their limitations, Ref. [6]. To get a good signal-to-noise ratio, high laser power and long acquisition times were needed. The recent improvements in lasers, spectrographs and detectors have made Raman spectroscopy a potential candidate for optical diagnostics of tissue. This chapter includes a summary of the equipment used for Raman spectroscopy, techniques for fluorescence rejection and a brief introduction to the Raman measurements in tissue that have been performed so far.

3.2 Equipment for Raman Spectroscopy

All Raman spectroscopy systems consist of a light source, a spectrometer and a detector. Often it is necessary to use some sort of filter to reject Rayleigh-scattered light. To be able to perform measurement in living tissue inside the body, one has to use a fiber to guide the laser light and collect the Raman signal. The advantages and problems with fiber probes are discussed in chapter 4.

The laser

According to Ref. [7], most early Raman measurements were made with Fourier-transform (FT) Raman spectrographs and Nd:YAG lasers operating at 1.064 μm. Some experiments were also made with diode lasers (red light excitation) and Ti:sapphire lasers with excitation in the infrared. It has been shown that excitation with 1.3 μm light gives a better fluorescence rejection than excitation with 1.064 μm. The sensitivity of CCD detectors decreases for long wavelengths and they can not be used for wavelengths longer than 1 μm. With a diode laser in the near infrared region (NIR) and a NIR-enhanced CCD detector, the sensitivity is several magnitudes better than with a FT Raman system with Nd:YAG excitation.

Today, high-power (0.5 W) diode lasers with wavelengths around 800 nm are available. Diode lasers have the advantages of being user-friendly, compact (small size) and reliable. The diode laser can be damaged by back-reflections and one therefore has to insert an optical diode after the laser. A Faraday isolator is a magneto-optic component that could be used with little loss. It consists of two polarisers with a permanent magnetic field in between. The first polariser has a transmission axis that coincides with the output polarisation of the diode laser. The angle between the transmission axes of the polarisers is 45° and the magnetic field turns the polarisation of the light this angle. Any back-reflection would be turned another 45° and extinguished at the polariser nearest to the laser

Laser cleaning filter

A laser does not produce perfectly monochromatic radiation since there can be weak non-lasing lines caused by spontaneous emission. This emission could cause artefacts in the measurements and has to be rejected with a narrow banded filter, for instance with a interference filter. There are also holographic band pass filters which work as a small dispersive component making it possible to block away unwanted lines with a small iris.

Laser rejection filters

To be able to measure small Raman shifts one has to have a good rejection filter that eliminates Rayleigh scattered laserlight that otherwise may give a high amount of stray light in the spectrograph. The filter should have a narrow region with high attenuation covering the laser wavelength and a high transmittance for all other wavelengths so that no small-shifted Raman peaks are reduced. This performance is found with volume-phase holographic filters, see Refs. [8, 9]. These filters consist of layers of varying refraction index, referred to as fringes. These layers are created by the interference between two mutually coherent laser beams that form a standing wave pattern, a hologram, in a medium. The medium is a dichromated gelatine (DCG) that has a large refraction index modulation capacity. After the recording, the hologram is processed to give varying density and correspondingly varying refraction index. The layers are separated by a length of $\lambda/2$, where λ is the wavelength of the recording beam. Only the wavelengths that fulfil the condition for Bragg diffraction will be reflected, i.e. the same wavelength as the recording wavelength, while all other wavelengths will be transmitted. The hologram is thick compared with the wavelength and it is placed between two glass plates for stability. The grainless nature of the gelatine gives very little scattering and high resolution, 5000 lines/mm. The filter is called notch filter and has optical densities from 4 to 6 at the rejection line. With a hologram thickness of 100 μm, Raman lines can be observed as close as 40-50 cm^{-1} from the laser line.

The spectrograph

One of the many limitations of Raman systems has been the throughput of the spectrograph. Spectrographs with a single reflection grating are insufficient to reject Rayleigh scattered light and give a lot of stray light, Ref. [7]. With double and triple grating spectrographs, the stray light can be rejected but the transmission is reduced to a few percent due to reflection losses and grating efficiency. The same technology used to produce holographic notch filters can be applied to produce high quality transmission gratings with high efficiency, excellent resolution, low scattering and high transmission, Ref. [10].

One example of a spectrograph with holographic transmission grating is the HoloSpec f/1.8i from Kaiser Optical Systems, Inc. With a holographic super notch filter the spectrograph will have a large throughput, ~50% (Ref. [7]), large light collection efficiency and be very compact with no moving parts. The optical layout of this on-axis holographic monochromator is found in Figure 3-1.

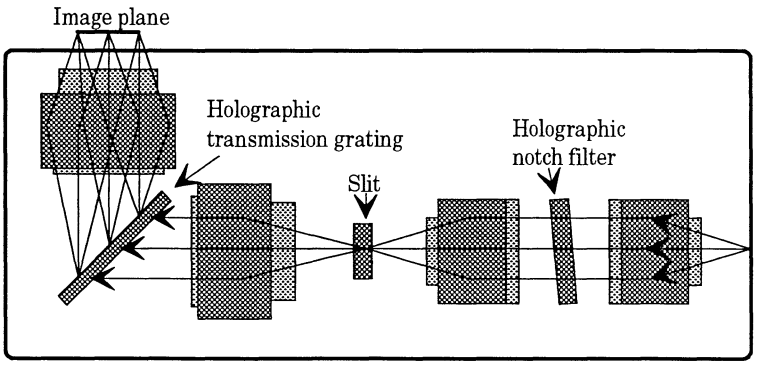

Figure 3-1 HoloSpec f/1.8i. Modified from Ref. [7].

Multi-element lenses are used on-axis as the collimating and focusing element and the dispersing holographical glass plate is placed in the collimated section. The 90° fold of the optical path and the high spatial frequency of the grating leads to high angular dispersion. With a 2 inch wide (25.4 mm) CCD chip, the system covers ~1900 cm^{-1}. The fact that the spectrograph has a very low f-number, f/1.8, means that it has a large acceptance angle and thus a high light gathering capability.

Fourier-transform spectrographs are used together with longer excitation wavelengths, e.g. Nd:YAG laser line at 1.064 μm. The spectrometer is a dual-beam interferometer of the Michelson type. The incoming light is dived into to paths by a beamsplitter, reflected at two mirrors and then joined again at the photodetector. When one mirror is moved, there will be a difference in the path length and the interference is recorded at the detector. This interferogram is the Fourier transform of the frequency spectra of the incoming light. The mirror has to be moved a long way in order to get a high resolution. More about the mathematical theory of Fourier-transform spectrographs can be found in Ref. [5].

The detector

For FT-Raman spectroscopy one can use a photoconductive detector that has a high sensitivity to infrared light compared with a photomultiplier that is commonly used for UV and visible spectroscopy. The conductivity of the sensor is increased since the photons absorbed in the semiconductor produce more electrons in the conduction band.

With a grating spectrometer one has two possibilities, either turning the grating and collecting the signal at one place or to use an array or matrix of small detectors that covers the spectra from the grating. The latter configuration has the advantage of collecting the whole spectrum simultaneously. Today, most detectors used are CCD (Charged Coupled Device) cameras. In order to get a spectrum from grating dispersed light, all rows in a column are added to a single value. The spectral resolution of a CCD is limited by the pixel size, not by the point spread function of the optics. With cooling, the shot noise level is very low. There are CCDs with Peltier cooling down to -45°C and others with liquid nitrogen cooling and added heating to -120°C. All liquid-nitrogen-cooled detectors must operate at a low pressure, ~10 mTorr, to prevent condensation and contamination of the CCD chip, Ref. [11]. CCD cameras can only be used for wavelengths shorter than 1 μm. There are ways to improve the sensibility. Back-illumination and special surface coatings increase the quantum-efficiency.

3.3 Fluorescence removal

The fluorescence from an interesting sample can be 10^6-10^8 times stronger than the Raman scattering. Below, there are a number of different spectroscopic techniques and computer analysis techniques that can suppress fluorescence and enhance the weak Raman signal. They are all based on one of the following three differences between fluorescence and Raman scattering:

- The lifetime of fluorescence is longer than the lifetime of Raman scattering.
- Raman peaks are narrow while fluorescence in general is broad-banded.
- Fluorescence is generally unpolarised but some Raman modes are strongly polarised.

Shifted Excitation Raman Difference Spectroscopy (SERDS)
By taking two spectra, with slightly different excitation wavelengths ($\Delta\lambda$~1 nm), the Raman peaks will be shifted but the fluorescence will look almost the same. By subtracting the two spectra the fluorescence is removed and the result is some sort of derivative of the Raman spectra. Integration of the difference spectra gives the Raman peaks, without any fluorescence. According to Ref. [12], Ramanpeaks that are 10^{-3} times weaker than the fluorescence background have been clearly and easily observed with this method.

Shifted-Spectra Technique
An easier way to get shifted spectra, if you are not the happy owner of a tuneable laser, is to make a software wavelength shift by simply shifting the spectra one pixel. If you are using a grating, you could move the grating a small amount and thus get two spectra. In either way, you will get two identical spectra, shifted a small amount, and then you proceed in the same way as with the shifted excitation technique. In order to get a Raman spectrum it is necessary to make a computer model of the difference spectrum.

Edge detection or First-Derivative Spectroscopy
When the fluorescence lines are broad it is easy to detect to Raman signal by taking the first derivative of the spectra. The narrow Raman peaks will get more distinguished than the broadbanded fluorescence. To get a large signal-to-noise ratio it is necessary to smooth the spectra. If the smoothing is done before the derivation, the signal intensity decreases, according to Ref. [13].

Shifted Excitation Raman Difference Spectroscopy, Shifted-Spectra Technique and Edge-Detection gives differential spectra. If no curve fitting is applied, it is difficult to analyse these spectra. In Ref. [13], they found out that the Shifted-Spectra technique had a better S/N ratio than the Edge-Detection technique since the latter subtracts adjacent points.

Fast Fourier Transform (FFT) with Highpass Filtering
A spectrum can be considered as a row of data and can be Fourier transformed into the spatial domain. The Raman peaks are sharp and give high spatial frequencies while the fluorescence varies slowly and hence yields low frequencies. The first term of the Fourier transform is a constant offset. Higher frequencies correspond to rapid variation, the Raman peaks. The convolution theorem states that a multiplication in the frequency domain is the same as convolution in the spatial domain. If the degrading from the slit in the spectrograph is known, one can compensate for this by making an inverse filtration and inverse transform. Unfortunately this process is sensitive to noise and the accuracy of which the slit function is known. Highpass filtering and inverse Fourier transformation gives the original spectra back without fluorescence. Random noise like cosmic particles causes high peaks with high spatial frequencies. Lowpass filtering will get rid of these.

Temporal Techniques
The lifetime of electronic states (10^{-7}-10^{-9} s) in molecules is longer than the lifetime of Raman signals (10^{-11}-10^{-13} s) since Raman scattering involves virtual energy levels. Using a short-pulsed laser and a fast time-gated detection system, one can detect the early photons (mostly Raman and little fluorescence) and reject the late fluorescence photons.

Another way is to modulate the laser intensity at a high frequency. If the fluorescence decay time is longer than the modulation period, it will not have any effect on the fluorescence signal. The Raman signal will however follow the modulation and can be

detected with a phase-sensitive lock-in detector, an electro-optic demodulator or a spectrum analyser.

A streak camera can also be used for fluorescence removal. The streak camera has higher time resolution than an ordinary single photon counting method using a photomultiplier, and has the two-dimensional capability of multichannel detection, both in the time domain and the spatial domain. In Ref. [14] they used the streak camera together with picosecond pulses and managed, with a proper time window choice, to extract the weak Raman signal from the strong fluorescence background. With this time-resolved technique, it is possible to study the temporal behavior of the Raman scattering process.

Polarisation modulation

Fluorescence is generally unpolarised while Raman scattering can be either polarised or unpolarised depending on the symmetry of the vibration mode. With polarised excitation light and a polarising analyser, the difference between the parallel and the perpendicular spectra will give a fluorescence-free detection of the Raman signal. Since not all Raman modes give polarised emission the method can not detect all peaks and in addition, the polarising analyser blocks half the signal.

Adding of a fluorescence quencher

Adding of a non-Raman active fluorescence quencher could suppress fluorescence but high concentrations may pertubate the sample. This is why this method is not used with biological samples.

Anti-Stokes Raman spectroscopy

There can be no fluorescence that hides the Anti-Stokes Raman signal, but on the other hand, the intensity of the signal is so weak that it is almost impossible to measure it.

Choice of excitation wavelength

The fluorescence background produced by most organic compounds is a broad envelop at longer wavelengths than the excitation wavelength. With UV or near-infrared excitation the fluorescence influence is reduced. All laser irradiation has the disadvantage of heating the sample. In addition, UV excitation has the disadvantages of being mutagenic to biological samples and it is hard to use UV radiation with fibers since most fibers have large transmission losses at short wavelengths.

With a longer wavelength, the energy is not enough to excite the lower electronic states and cause fluorescence. However the intensity of the Raman scattering has an $1/\lambda^4$ dependence which means that the signal gets weaker as the excitation wavelength gets longer.

Polynomial Fit

Fitting a polynomial of high enough order to describe the slowly varying fluorescence background and low enough not to follow the sharp Raman peaks to a recorded spectrum and then subtract the polynomial fit from the spectrum could eliminate some fluorescence. This method can not be used for rejection of fiber background though, since this background has peaks.

3.4 Tissue Diagnostics by Raman Spectroscopy

Medical diagnosis by optical spectroscopy has been done with fluorescence for a long time with good results in many areas. The method is used for detection of cancer and precancer lesions in the breast, lung, bronchus, oral cavity, cervix, and gastrointestinal tracts, Ref. [6]. A drawback of fluorescence is that only a few biological substances such as flavins, porphyrins, and structural proteins (collagen and elastin) have distinct fluorescence peaks and often the bands overlap each other. On the other hand, most substances are Raman active and Raman spectroscopy offers in many ways a more distinct classification of tissue. Raman spectroscopy probes the individual vibration energies in molecules corresponding to single atoms or small groups and thus Raman peaks are narrower than fluorescence. According to Ref. [6], inflammations could in fluorescence spectroscopy look almost the same as precancerous areas but Raman spectroscopy may yield an unambiguous result.

UV-Raman spectroscopy has been used for a long time for the diagnosis of tissue *in vitro*. With short enough wavelengths, the energy of the UV light does not correspond to the absorption bands of the tissue and fluorescence is reduced. This can not be done *in vivo* since the UV radiation may be mutagenic. With longer wavelengths in the near infrared region the tissue fluorescence is smaller but in the past, the lack of detectors in the near infrared region made Raman spectroscopy impossible. Today there are low-noise, cooled, near-infrared enhanced CCD detectors and compact, powerful diode lasers.

When dealing with all kinds of optical spectroscopy it is important that the tissue does not get heated too much. At 60°C the proteins start to denaturate and at 100°C the water in the cells start to boil and the cells die. At 300°C the cells will be carbonised. Already at 42°C the tissue starts to get damaged and thus it is important to keep track of the laser-induced heat.

The choice of wavelength is important since it affects the penetration depth. In tissue there is an absorption window in the infrared between approximately 700 nm where the absorption of the blood decreases and 2 μm where the absorption of the water increases. In this region, the penetration depth can be as large as 4-5 mm.

Another aspect is the collection time. In regions where there are a lot of movements, e.g. in the heart region, one can not collect for more than a few seconds when using a fiber *in vivo*.

Many groups have measured on pure tissue components (proteins, lipids, collagen, ATP, NADH, elastin etc.) and on tissue samples taken from the body as biopsies, *in vitro*. For biopsy samples, it is necessary to interrupt the metabolism and stabilise the tissue. This fixation can in some cases alter the Raman spectra and introduce spectral artefacts. Different fixation methods like tissue drying, formalin fixing, snap freezing, tissue freezing in optimal cutting temperature (OCT) and extended post-thaw, were investigated in Ref. [15]. Freezing at -85°C and thawing in room temperature would give the best results, i.e. least artefacts. To be able to make *in vivo* measurements, the use of fiber probes is necessary. More on this topic is found in chapter 4.

One also has to have some sort of algorithm that automatically distinguishes between the spectra from normal and diseased tissue. This algorithm can be based on the presence, location and intensity of a peak, a ratio between two peaks or a more complex expression. The use of neural networks or principal component analysis are two more methods.

4. Background to Fiber-Optical Raman Spectroscopy

4.1 Introduction

Fibers offer an easy way to measure at awkward places like hostile environments and at otherwise unapproachable sites, for instance inside the body. Unfortunately, scattering in the fibers can hide weak signals like Raman scattering. There are some different techniques to reduce the fiber emission. During the collection of the Raman signal it is possible to use different probes that reduce the fiber fluorescence, one fiber for excitation and one or many for collecting the signals. Another way is to use filters after the excitation fiber and before the collecting fiber(s). One can also use the different spectroscopic techniques and computer analysis that are described in 3.3. The removal of the fiber background with the aid of computer analysis is more complicated than removing a simple increased fluorescence background since the fiber background is structured and contains Raman peaks.

4.2 Introduction to the basic concepts of fiber optics

A fiber consists of a transparent, homogenous core, where the light is guided. The core is surrounded by a homogenous cladding. The refraction index of the core is larger than the index of the cladding and in Figure 4-1 there is a schematic picture of a fiber.

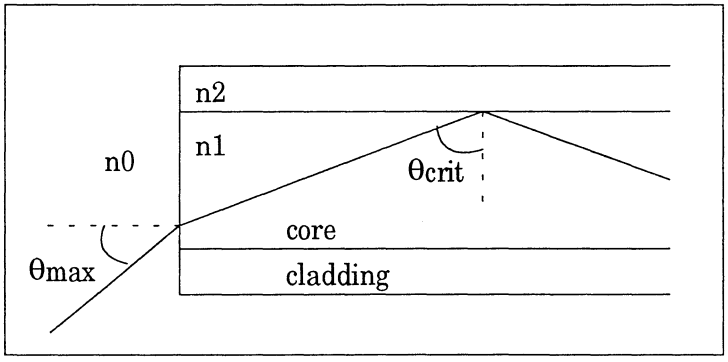

Figure 4-1 Light refraction and reflection in fiber.

According to Snells law, there will be totally internal reflection when the incident angle θ_{crit} is larger than $\arcsin(n_2/n_1)$ where n_2 is the refraction index for the cladding and n_1 is the refraction index of the core.

$$\sin(\theta_{crit}) = \frac{n_2}{n_1} \tag{4.1}$$

The maximum launching angle (θ_{max}) or acceptance angle is determined by

$$n_0 \sin(\theta_{max}) = n_1 \sin(90 - \theta_{crit}) \tag{4.2}$$

where n_0 is the refraction index of the surrounding media. The left hand term is called the numerical aperture, NA.

$$NA = n_0 \sin(\theta_{max}) = \sqrt{n_1^2 - n_2^2} \tag{4.3}$$

Should the incident angle be greater than the acceptance angle, θ_{max}, the requirements for total reflection are not fulfilled and some of the light will leak out into the cladding. Fibers are often made of silica and therefore they are fragile and need a plastic protection layer around them. The plastic layer may prevent external light to pass through the cladding and get coupled into the core.

Most fibers are multimode-fibers, which means that the light can propagate in many different paths, some almost straight and some with many reflections along the way, see Figure 4-2.

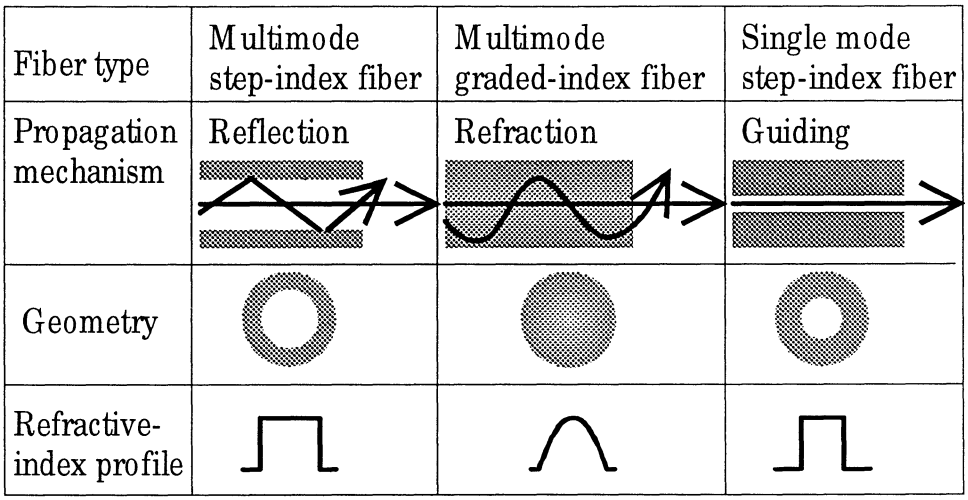

Figure 4-2 Different fiber types. Modified from Ref. [16].

In single mode fibers the light can only go straight forward. There are two kinds of multimode fibers, one with two different indices for core/cladding, the step-index fiber, and one with a gradual change between the refraction indexes, the graded-index fiber. In the step-index fiber, the light that undergoes many reflections will have a longer way than the light that travels straight which makes pulses longer. With the graded-index fiber the optical path is the same for all ways since the light that travels along the edges experiences a higher refraction index. With this fiber, pulses retain their original length.

There will always be some loss of light when you are using fibers. The guiding of the light into the fiber is a critical point. One have to use a lens that matches the acceptance angle of the fiber and a x-y-z positioner to optimise the coupling. If the incident angle is too large, the light will not undergo total reflection at the surface between core and cladding but will leak out through the cladding. Beside this misalignment, there is always some attenuation caused by impurities in the core that will scatter and absorb the light. This attenuation is measured in dB. The attenuation expressed is $10*\log(P_{in}/P_{out})$ where log is the tenth logarithm, P_{in} is the effect at the beginning of the fiber and P_{out} is the effect at the end of the fiber. The damping is often given in dB/km.

Fibers offer a certain amount of flexibility but if they are bent too much, the condition for total internal reflection is not fulfilled and light leaks out in the cladding. If the fiber is bent any further, the core could break and the transmission would decrease to almost nothing.

4.3 Fiber Emission Background

The fiber background from silica fibers consists of a fluorescence baseline and some broad Raman peaks, see Figure 4-3..

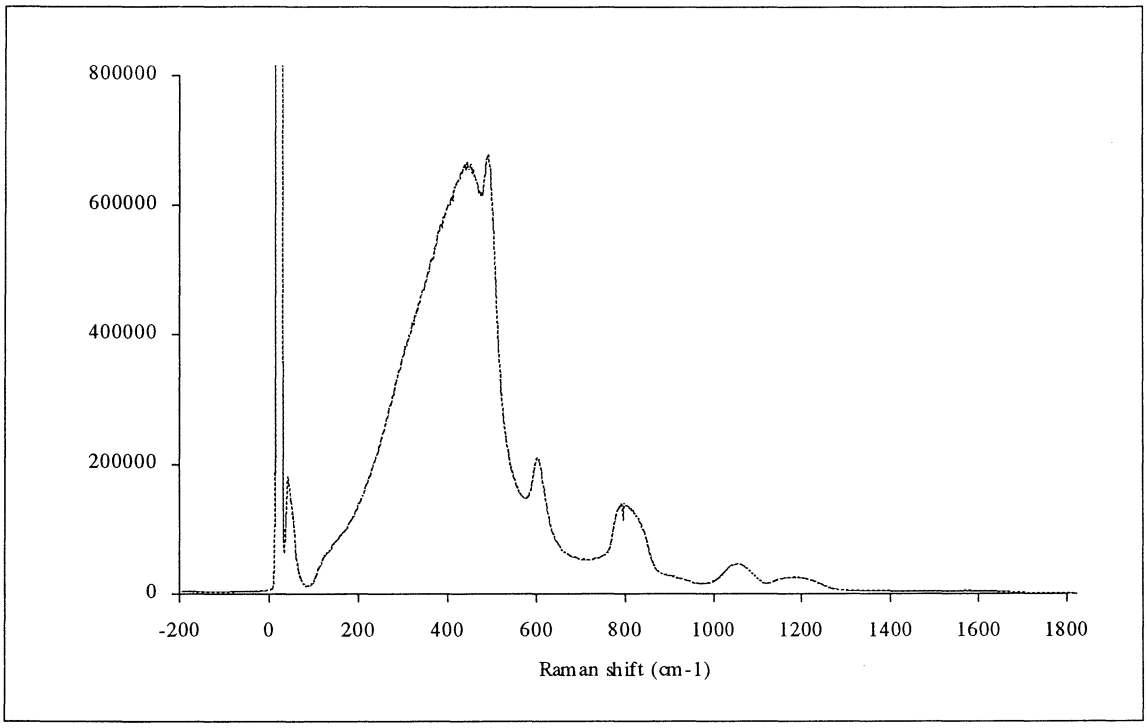

Figure 4-3 Fiber emission from an Anhydroguide fiber (Fiberguide Industries, Inc.) after 785 nm excitation.

According to Ref. [17], the fluorescence baseline comes from light that has escaped into the cladding and the plastic protection layer. Impurities in these layers will cause fluorescence. The molecules in the plastic protection layer can also cause some relatively narrow Raman peaks, like the C-H stretching mode. This peak is at ~3000 cm^{-1} and thus not visible in the figure. The core gives broad Raman peaks, clearly visible in the figure. Raman scattering from the core originate from the whole length of the fiber while the fluorescence comes from points where the light escapes from the core, according to Ref. [17]. Improper launching, misalignment and sharp fiber bends cause more losses into the cladding/plastic protection layer and hence a higher fluorescence background.

4.4 Different Probe Configurations

It is important to get a large overlap between the excitation and collection volumes and thus a large signal-to-noise ratio. Obviously, the best way to get a good collection efficiency is to make sure that the excitation area and the collection area overlap perfectly. This is also the easiest way to measure, using a single fiber that has been cut and polished at the end. On the other hand, this way gives a large fiber background that can hide weak

signals. In order to decrease the background, many groups have tried different probe configurations with two or more fibers. A more complete summarise of different probe configurations can be found in Ref. [18].

4.4.1 Dual-Fiber Probes

In Refs. [17, 19] they used two fibers, one fiber that led the excitation light and one that collected the scattered light. They investigated two different arrangements, one where the fibers were held together beside each other, see Figure 4-4a, and one with the fibers opposite each other, a so called Optical Fiber Facing (OFF) configuration, see Figure 4-4b.

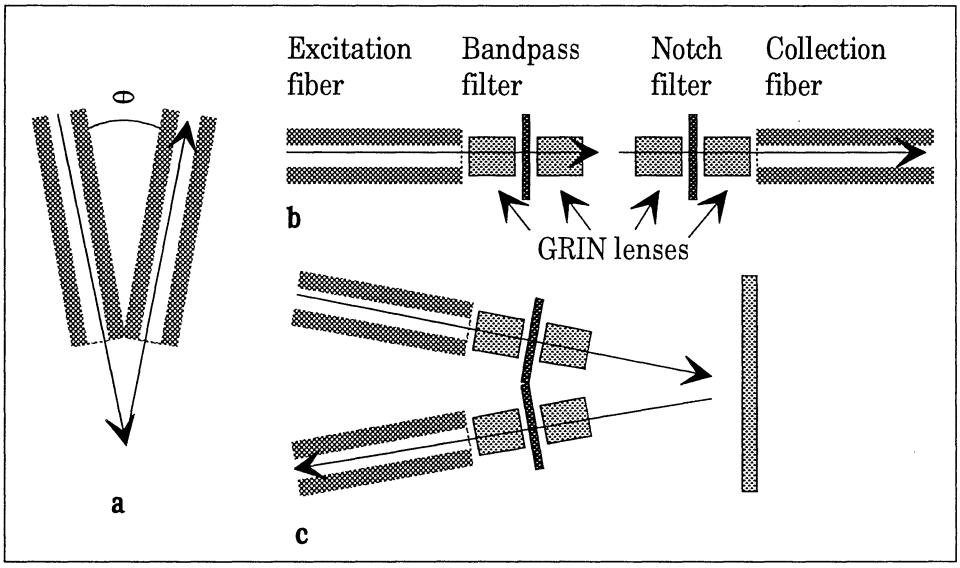

Figure 4-4 Different probe configurations. Modified from Refs. [17, 19].

With the two fibers parallel to each other or with some angel between, the sensitivity was increased when there was a collimating graded-index-lens (GRIN) at the end of each fiber. For small angles, 0°-15°, between the fibers, there was an overlap between the excitation and collection volumes and thus high sensitivity. Greater angles decreased the overlapping volume. For the OFF -configuration measurements, filters were used at the ends of the fibers, between the GRIN lens and the sample. Bandpass interference filters were used to "clean up" the excitation light and a longpass interference filter was placed in front of the collection fiber in order to suppress scattered laser light. This arrangement gave almost no background emission, even with 250 meters long fibers. The OFF arrangement presupposes that the sample is transparent like a fluid or a gas, but in the case of a solid opaque sample, the fibers must both point at the surface with some angle between, see Figure 4-4c. With this configuration they got almost the same good result as the configuration with the fibers pointing towards each other. The conclusion was that the OFF configuration had a larger collection efficiency than two fibers without any filters.

In Ref. [20], they came to almost the same conclusions when measuring on a sensing plate tip having silver-coated microparticles deposited on a glass support. The method is called Surface Enhanced Raman Spectroscopy (SERS).

Another way is to arrange the fibers parallel and close to each other. If the ends of the fibers are cut at an angle, it is possible to get better overlap between excitation and collection than with plane fiber ends.

An alternative way is to use a lens to couple the Raman scattered light into the collection fiber. The main drawbacks with this method are the lens fluorescence, reflection losses, energy absorption and photodegradation when high laser powers are used, Ref. [18].

4.4.2 Multiple-Fiber Probes

The first attempts with multiple fibers were made with a fiberprobe with one fiber bundle for excitation and one for collection. This proved to be inefficient since a lot of radiation escaped to the cladding or to the material surrounding the fibers. The next idea was to have one excitation fiber surrounded by several collection fibers. This geometry is called n-around-1 where n stands for the number of collection fibers. The major disadvantage of the multiple-fiber probe is the cost of long fibers and the high levels of fiber emission.

In Ref. [21] they used a multifiber probe for Raman measurements in liquids. The probe contained 19 collection fibers around the central excitation fiber. The collection fibers were coupled to a linear array spectrograph. When the probe was immersed in clear liquids or placed at an 45° angel to a solid sample, the results were good and with little fiber background. With highly scattering liquids and normal excitation and detection of solid samples, the fiber fluorescence was severe. Proper filtering could minimise this problem.

4.4.3 Filtered Mono-Probes

The use of a single fiber has the advantages of a perfect collection geometry and an easy way of use, but gives high levels of fiber emission for long fiber lengths. The dual fiber probe has a lower collection efficiency and is more difficult to align properly but gives less fiber emission in the spectra. By making a hybrid of these two, it is possible to get a better probe. The idea is to guide the excitation light to the measuring place through a long fiber, filter with a narrow bandpass filter to get rid of the fiber emission and launch the cleaned laser light into a short fiber. The sample emission would go back through the short fiber and before it is directed into the long collection fiber, it is filtered again, this time with a notch filter. The filter removes any Rayleigh scattered laser light that could have caused fiber emission on the way back to the spectrograph.

The OFF configuration described in Ref. [17] was good for measuring liquid samples but not for solid ones and the angled configuration was difficult to align. With the same filtering but with a coaxial set-up the handling is much more easy. There have been numerous versions of coaxial probe which all uses a dichroic mirror of some kind. The main principle is shown in Figure 4-5.

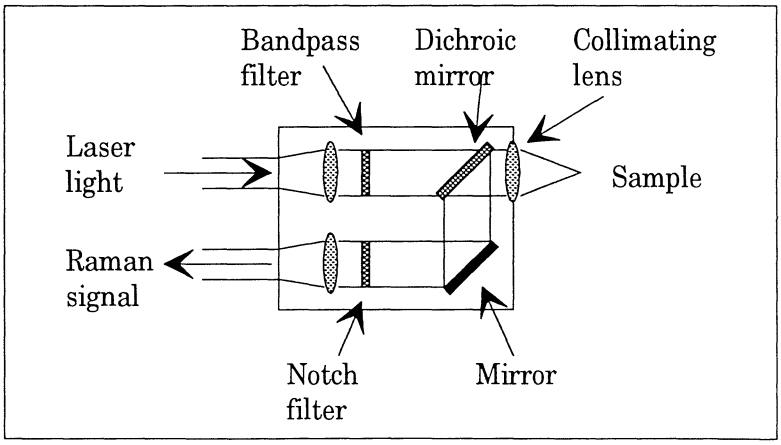

Figure 4-5 Coaxial filtered probe.

There is a commercial coaxial filtered probe (Super Head, Dilor Corporation) that has been evaluated in Ref. [22]. The probe contains an angle-tuned holographic Super Notch filter that was used instead of the dichroic filter in previous designs. They used the probe for concentration measurements of benzene/heptane solutions with good results. The spectra were mean centred (the mean spectrum was subtracted from each spectrum) to minimise the influence of the variation of the fiber emission. Some of the spectra were also mean shifted (the mean intensity of the useful part of the spectrum was subtracted) in order to take care of the intensity offset. With these methods, the real concentrations and the measured ones had an almost total correspondence.

In Figure 4-5, the sample is placed close to the probe but with a short fiber connected to the output, one can guide the light and measure at awkward places, e.g. inside the body. This configuration with a short bidirectional fiber is called a partially filtered probe since there can be some fiber emission that is not rejected by the longpass (notch) filter. This residual silica background may be subtracted by using a spectrum measured with a mirror or a diffuse reflector, such as potassium chloride, at the end of the fiber.

5. Fiber Emission and Transmission Measurements

5.1 Introduction

In order to build a fiber-optical probe for near-infrared Raman spectroscopy, it is important to use a fiber with high transmission and little fiber emission, see chapter 4.3. Since the Raman signal is weak, a strong fiber emission could hide the Raman signal from a sample.

Four different fiber types were tested and evaluated in order to get an idea of what fiber to use. The fibers were 8 meters long and for each fiber, two different core diameters were tested (400 μm and 600 μm). For the fiber emission measurement, a strong Raman scatterer, Rhodamine 6G, was used as a test object. The ratios between seven Raman peaks and their fiber emission background were used as a measure of suitability. A power meter was used for the transmission measurement.

5.2 Experimental Set-Up for Fiber Emission Measurements

The experimental set-up can be seen in Figure 5-1.

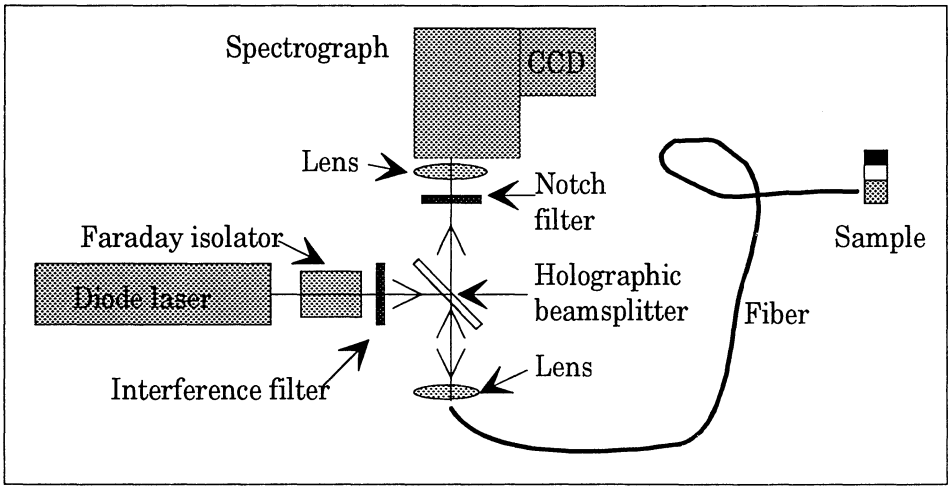

Figure 5-1 Experimental set-up for fiber emission measurements.

The laser was a diode laser (SDL-8630 Tuneable CW Laser Diode), with a maximum power 0.5 W at $\lambda = 785$ nm. With a motion controller (Motion Master 2000, Newport) that moves a grating inside the laser cavity, the laser is tuneable in a short interval, 781-795 nm. A Faraday isolator (Electro-Optical Technology Inc.) was inserted directly after the laser in order to prevent any back reflections to get coupled into the laser cavity and damage the laser.

The light out from the laser contained some unwanted emission at slightly longer wavelengths than the laser line, between 0 and 150 cm^{-1} from the laser line. This emission was reduced with a narrow-banded interference filter (Omega Optical Inc.) in order not to get any artefacts in the measurements. The light was further guided with a holographic beamsplitter (Kaiser Optical Systems, Inc.) and a lens into an 8 meter long fiber. The fiber was cut and polished at the ends. The distal end was directed into the air for pure fiber emission measurement and perpendicularly onto a small glass cylinder containing Rhodamine 6G for the Raman measurements. Rhodamine 6G is a dye often used in dye

lasers. Some of the scattered light (Rayleigh light and in the case of Rhodamine also Raman-scattered light) was collected by the fiber end and led back through the fiber.

The holographic beamsplitter transmits (>80%) light with wavelengths longer than 350 cm^{-1} red-shifted from 785 nm and reflects the light (>90%) at λ = 785 nm. The Raman scattered light (from the sample and the fiber itself) and some Rayleigh-scattered light is thus transmitted. To reduce the rather uninteresting Rayleigh scattered light and avoid stray light in the spectrograph, a notch filter (Super Notch Plus, Kaiser Optical Systems, Inc.) was placed in front of the spectrograph. In the spectrograph (Holospec f/1.8i, Kaiser Optical Systems, Inc.), which is further described in chapter 3.2., the light is collimated by near-infrared anti-reflection coated lenses, filtered by a notch filter and then refocused onto the entrance slit (25 μm wide) of the spectrograph section. The light is then collimated again, passed trough the holographic grating and focused onto a flat image plane coincident with the plane of the CCD detector. The linear dispersion of the grating was 4.6 nm/mm and together with the 1 inch (25.4 mm) wide CCD chip, it gave a spectral coverage of -190 - 1850 cm^{-1}.

The light was detected with a back-illuminated, near-infrared-enhanced, nitrogen-cooled CCD camera (LN/CCD-1024 EHRB, Princeton Instruments, Inc.) The CCD chip can not distinguish between optical photons and high energetic cosmic particles which give rise to narrow high intensity peaks in the spectra. The computer software (WinSpec) can reject these cosmic particles in two ways, spatially or temporally, see Ref [23].

The peak removal is applied to newly collected data, after it is received by the computer but before it is stored. A cosmic peak has a much higher intensity than the surrounding pixels and can hence be rejected spatially. The software generates a second derivative of the pixel intensities and removes points exceeding a certain threshold. The peak is removed and replaced by a the linear interpolation of the two neighbouring pixels. Temporal cosmic ray removal requires a series of spectra. The cosmic particles appear very quickly and can thus be removed by comparing the intensity of each pixel with corresponding pixel in the previous spectrum. The pixel intensity in the second spectrum is replaced by the minimum of the two intensities. In these measurements, temporal rejection of cosmical particles was used.

The wavelength calibration (pixel-wavelength) was made with a neon spectral lamp. A spectrum of the hydrocarbon indene (C_9H_8) was used for Raman calibration. This spectrum has many peaks in the 500-1600 cm^{-1} region which have been accurately measured, see Ref. [24]. No intensity correction due to the quantum efficiency variation with respect to wavelength of the CCD chip was made.

The different fibers were Anhydroguide (low OH content) and Superguide from Fiberguide Industries, Inc. and two fibers from ANDA (Lithuania), one normal and one with low OH content. For each fiber, two different core diameters (400 μm and 600 μm) were tested.

5.3 Results and Discussion of Fiber Emission Measurements

The fiber emission and Raman peaks were measured for all fibers and core diameters. The laser power was ~170 mW and the power out from the fiber was ~40mW, in all measurements. The total acquisition time was 10 seconds in each spectrum.

The fiber emission from an 8 meter long, 600 μm core diameter, Anhydroguide fiber can be seen in Figure 5-2.

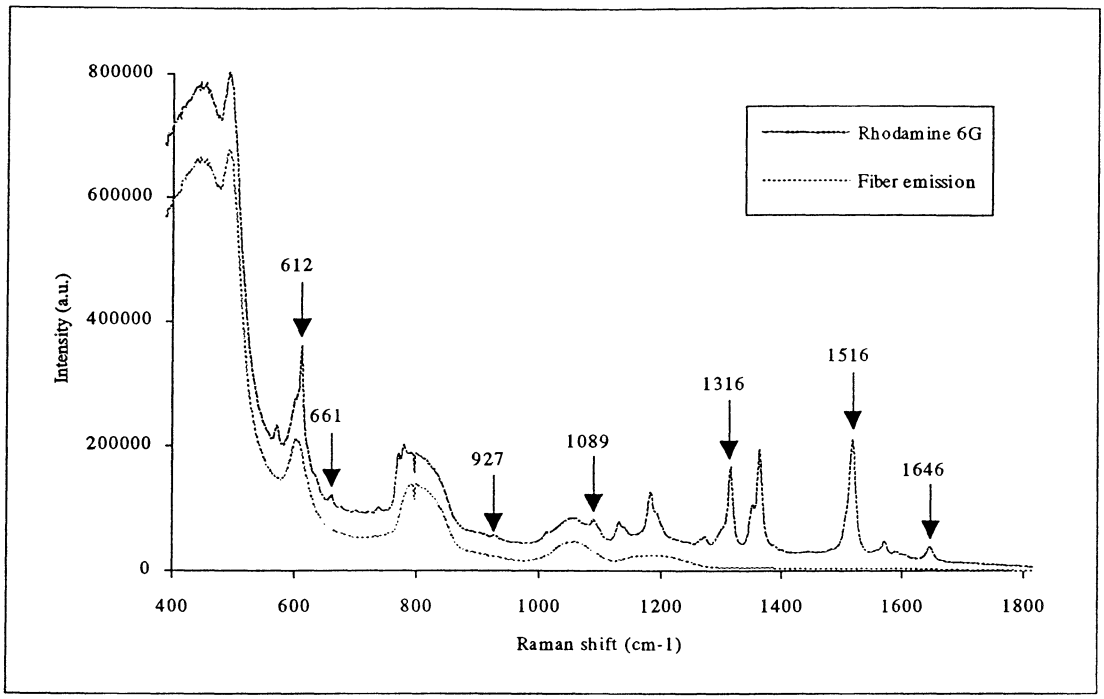

Figure 5-2 Fiber emission from the Anhydroguide fiber and fiber emission + Raman signal from Rhodamine 6G.

There are two curves in the figure, one with Rhodamine 6G placed in front of the fiber end and one with pure fiber emission acquired when the fiber was pointing out in the air. The Raman peaks from Rhodamine 6G lie on top of the fiber emission curve. As described in chapter 4.3, the fiber emission consists of fluorescence and Raman peaks from impurities in the core, cladding and the plastic protection layer. The seven peaks indicated with arrows in Figure 5-2 were used to evaluate the fibers. For each peak, the ratio between the height of the Raman peak and the fiber background was calculated according to Figure 5-3.

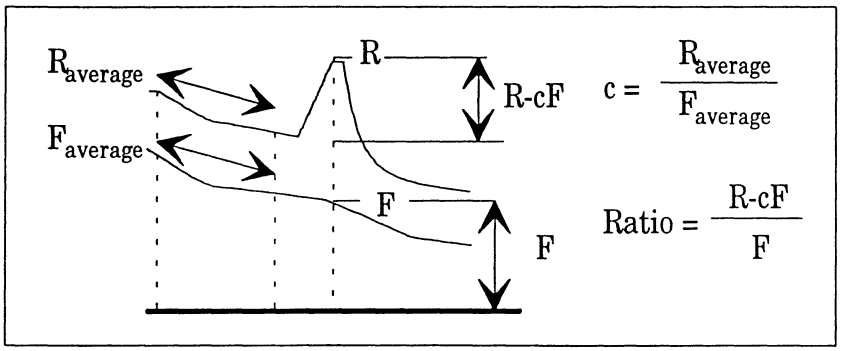

Figure 5-3 Formulas for calculating the ratio between a Raman peak and it's fiber emission background.

In order to get the amount of fiber emission under the Raman peak, an average of five pixels were calculated for each curve some pixels away from the peak. This gave a factor c, that describes the increased fiber emission background under the peak. The pure Raman emission can now be "lifted off" the background. The ratio between the Raman peak and it's fiber emission background can then be calculated. This was done for all fibers and the

ratios can be found in Table 5-1 and Table 5-2. In Figure 5-4 and Figure 5-5, all measurements with Rhodamine 6G and 600 μm and 400 μm core fiber, respectively, are presented.

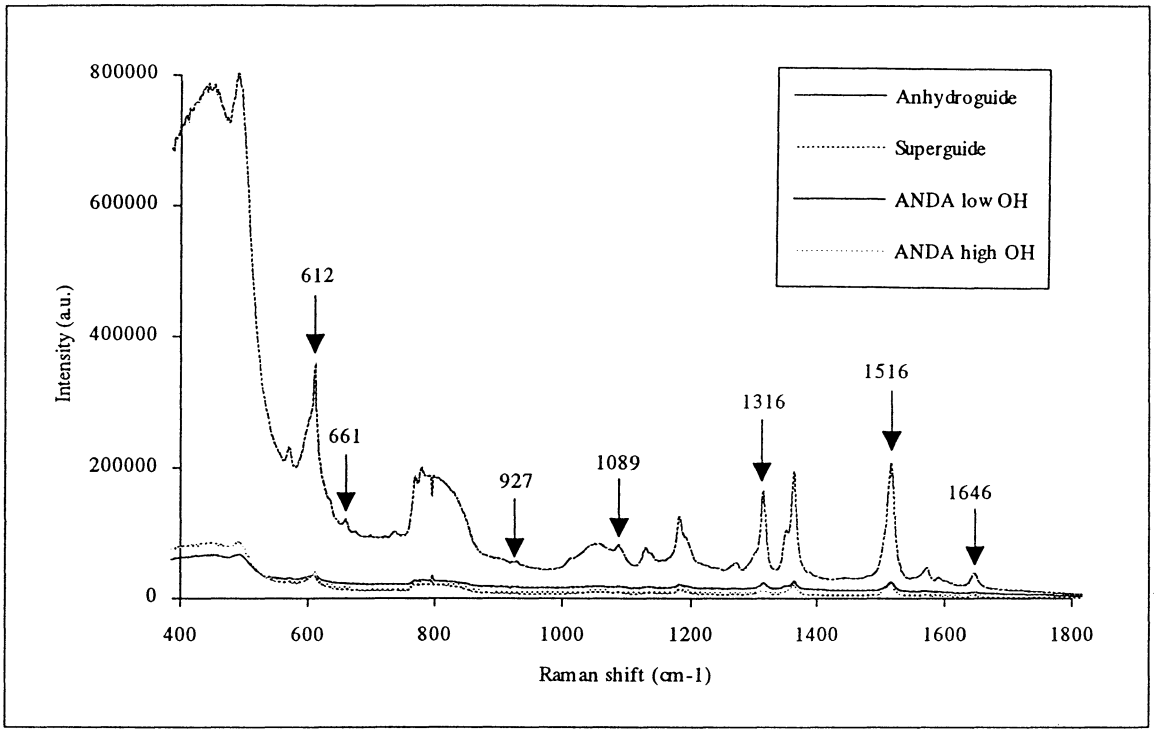

Figure 5-4 Fiber emission and Raman peaks from Rhodamine 6G for four different 600 μm core fibers.

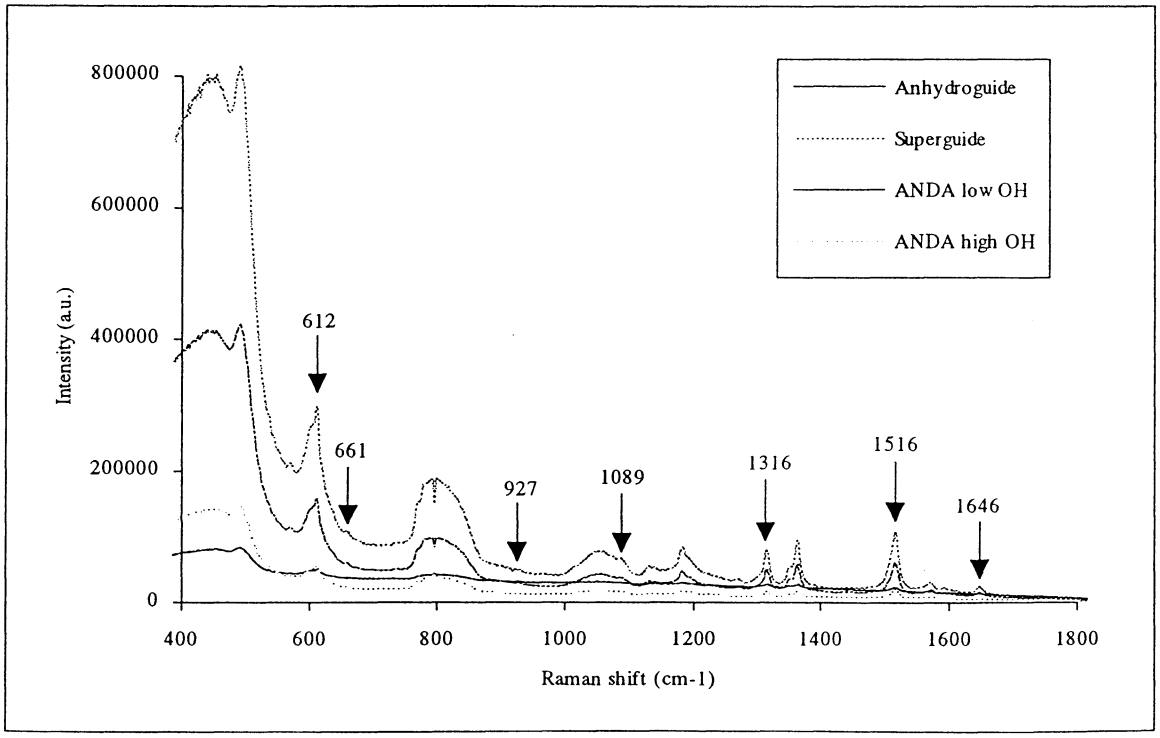

Figure 5-5 Fiber emission and Raman peaks from Rhodamine 6G for four different 400 μm core fibers.

Raman shift (cm^{-1})	Anhydroguide 600 µm	Superguide 600 µm	ANDA low OH 600 µm	ANDA high OH 600 µm
627	**0.627**	*0.503*	0.361	0.461
661	**0.305**	*0.250*	0.081	0.134
927	*0.057*	**0.064**	0.010	0.044
1089	**0.814**	*0.614*	0.116	0.226
1316	**27.071**	*5.386*	0.937	1.892
1516	**43.860**	*10.618*	1.612	3.938
1645	**5.110**	*1.367*	0.270	0.584

Table 5-1 Ratios between Raman peaks and their fiber emission background for different fibers and peaks. Numbers in boldface indicate the strongest ratios and the ones in italics indicate the second strongest ratios.

Raman shift (cm^{-1})	Anhydroguide 400 µm	Superguide 400 µm	ANDA low OH 400 µm	ANDA high OH 400 µm
627	*0.279*	**0.286**	0.080	0.163
661	**0.164**	*0.143*	0.018	0.067
927	-0.028	*0.014*	*0.014*	**0.025**
1089	**0.464**	*0.376*	0.010	0.116
1316	**9.474**	*8.790*	0.201	1.215
1516	**13.242**	*12.851*	0.338	2.138
1645	*1.606*	**1.650**	0.052	0.325

Table 5-2 Ratios between Raman peaks and their fiber emission background for different fibers and peaks. Numbers in boldface indicate the strongest ratios and the ones in italics indicate the second strongest ratios.

The bold numbers indicate the strongest ratios and the ones in italic the second strongest ratios for every peak. In Table 5-1, it is obvious that Anhydroguide is the most suitable fiber. The peak at 927 cm^{-1} is very weak and hence the ratios at 927 cm^{-1} are uncertain and, in the case of 400 µm fibers, the ratio was even negative which indicates an overestimated fiber emission background. In Table 5-2, the best choice is not obvious. Ignoring the ratio at 927 cm^{-1}, the ratios for the Superguide and the Anhydroguide are almost the same with a small advantage for the Anhydroguide. Note that the ratios for the ANDA fiber with low OH content are smaller than the ratios for the normal ANDA fiber which was unexpected.

5.4 Experimental Set-Up for Fiber Transmission Measurements

The experimental set-up can be seen in Figure 5-6.

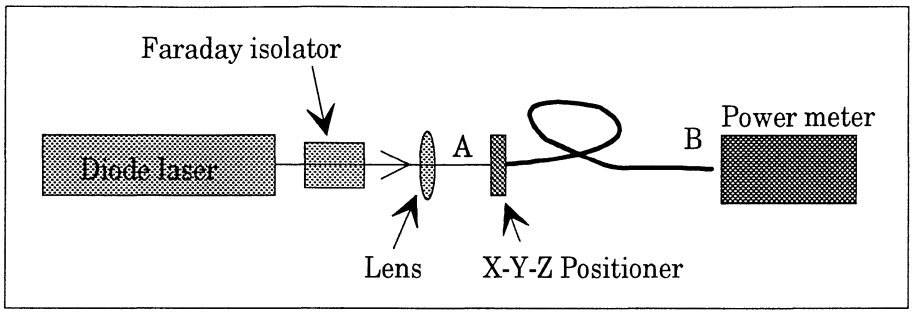

Figure 5-6 Experimental set-up for fiber transmission measurements.

The laser and Faraday isolator are the same as in the previous measurements. The light was focused into the fiber by an ordinary lens. The intensity of the light was measured with a power meter which gives the intensity in watts. The indicated powers can not be trusted for absolute measurements, only relative measurements are possible. The transmission is given by the ratio I_B/I_A where I_A and I_B stand for the intensities at point A and B respectively. I_B was measured for all fibers but I_A was only measured once per four fibers since the alligned X-Y-Z positioner had to be removed for I_A measuerments. The laser do not maintain a constant output power. The indicated laser power I_L on the laser controller therefore has to be considered when calculating the transmission ratio.

5.5 Results and Discussion of Fiber Transmission Measurements

In Table 5-3 and Table 5-4 below, the measured intensities and calculated transmission for each fiber are presented.

Fiber transmission measurements core diameter = 400 μm I_A = 95 mW when I_L =139 mW			
Fiber	I_B (mW)	I_L (mW)	Transmission = $\frac{139}{95}\cdot\frac{I_B}{I_L}\cdot 100$
Anhydroguide	75	132	83.1%
Superguide	75	133	82.5%
ANDA low OH	32	130	36.0%
ANDA high OH	20	135	21.7%

Table 5-3 Fiber transmission for fibers with core diameter 400 μm.

Fiber transmission measurements core diameter = 600 µm I_A = 85 mW when I_L =126 mW			
Fiber	I_B (mW)	I_L (mW)	Transmission = $\frac{126}{85} \cdot \frac{I_B}{I_L} \cdot 100$
Anhydroguide	70	125	83%
Superguide	72	126	84.7%
ANDA low OH	60	126	70.6%
ANDA high OH	52	125	61.7%

Table 5-4 Fiber transmission for fibers with core diameter 600 µm.

There was no clear difference between the transmission ratios of the Superguide fiber and the Anhydroguide fiber. The ANDA fibers have a very low transmission, the one with high OH being extremely bad. The launching of the light into the fiber and the uncertaincy of the power meter are two sources of errors.

5.6 Conclusion

In the fiber emission measurements it was found that the Anhydroguide fiber was the best choice among 400 µm fibers and equal to the Superguide fiber in the measurements of 600 µm fibers. The fiber transmissions of the Anhydroguide fiber and the Superguide fiber were equal.

In both measurements there are many sources of errors. Considering these sources of errors, the final conclusion must be that the Anhydroguide is the most suitable fiber for near-infrared Raman spectroscopy. Unfortunately, the inexpensive ANDA fibers were not a good alternative at all.

6. Probe Design

6.1 Introduction

In the previous chapter, it was established that the Anhydroguide was the most suitable fiber for near-infrared Raman spectroscopy. The next step was to test and evaluate different probe configurations on the optical bench.

The first configuration uses the same idea as discussed in chapter 4.4.3, i.e. a filtered coaxial probe with a holographic beamsplitter that reflects the laser light into the short measuring fiber. The other configuration excludes the holographic beamsplitter and instead uses a different launching angle for the excitation light, at the edge of the acceptance angle.

Rhodamine 6G was used as test sample and the evaluation was done by calculating the signal-to-noise ratio for the strongest Raman peak, 1516 cm^{-1}. For each set-up, the signal-to-noise ratio was calculated for five different laser powers and three different acquisition times.

6.2 Experimental Set-Up

The experimental set-up for the first probe configuration can be seen in Figure 6-1.

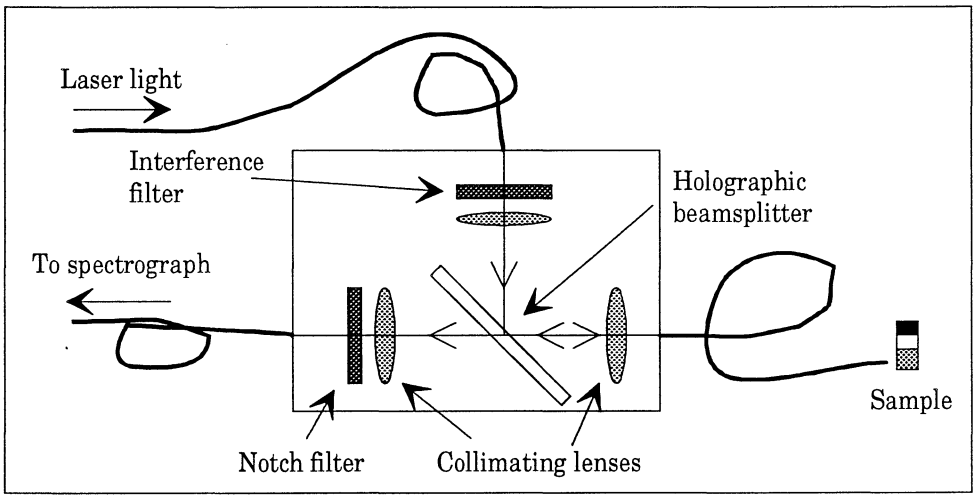

Figure 6-1 Probe configuration 1.

The equipment used was the same as in the fiber emission measurements. The laser light was guided from the laser, through the interference filter, collimated by a lens, reflected by the holographical beamsplitter and focused into the measuring fiber. The measuring fiber should be short, but in these measurements an 8 meter long Anhydroguide fiber was used. The fact that this long fiber gave much unwanted fiber emission did not matter for this evaluation since the same fibers were used in both probe configurations.

Like in the previous measurements, the test sample was Rhodamine 6G. The scattered light went back through the measuring fiber, was collimated by a lens, went through the holographic beamsplitter, was filtered by a notch filter and focused into the collection fiber which was coupled to the spectrograph with a special fiber connector.

The other probe configuration was quite different from the first one since the holographic beamsplitter was excluded. Instead, the excitation light was launched into the measuring fiber at an angle that was slightly smaller or the same as the acceptance angle of the fiber, see Figure 6-2.

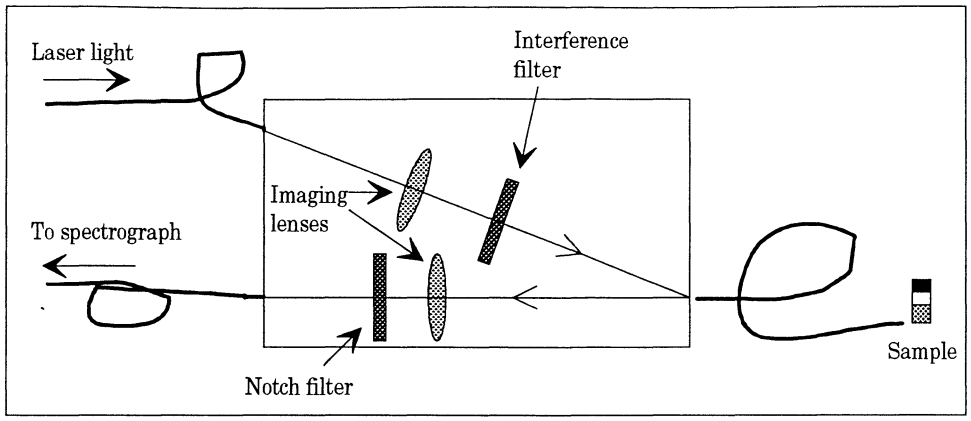

Figure 6-2 Probe configuration 2.

In this way, the measuring fiber was underfilled, i.e. the light in the fiber was only travelling around the edge of the fiber. This could be seen as a circle-shaped emission from the distal fiber end. The lenses were adjusted so that they gave an 1:1 magnification from one fiber end to next fiber end.

6.3 Results, Discussion and Conclusion

Each probe was tested with five different laser power intensities and three different acquisition times. For each measurement, the signal-to-noise ratio for the strong Raman peak at 1516 cm^{-1} was calculated according to Figure 6-3.

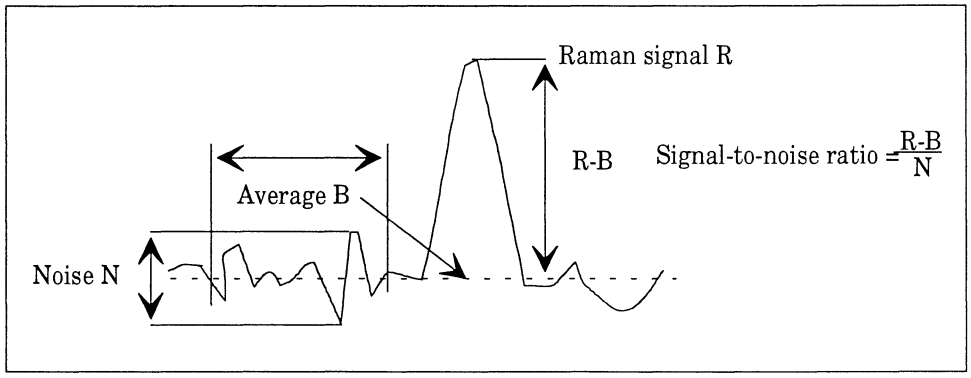

Figure 6-3 Formulas for calculating the signal-to-noise ratio.

The average background and the noise level were calculated from 21 adjacent pixels, some pixels away from the peak. The signal-to-noise ratios for the two probe configurations are presented in Table 6-1 and Table 6-2.

Probe configuration 1			
Laser power	Acquisition time		
mW	0.1 s	0.5 s	1.0 s
~124	21.8	58.6	94.5
~135	33.2	52.0	81.3
~160	24.5	60.9	63.9
~190	34.2	66.4	90.8
~245	44.0	64.1	82.3

Table 6-1 Signal-to noise ratios for probe configuration 1.

Probe configuration 2			
Laser power	Acquisition time		
mW	0.1 s	0.5 s	1.0 s
~121	5.2	16.5	23.4
~135	4.8	16.1	49.4
~164	6.2	14.2	35.0
~185	7.4	32.3	27.7
~243	11.4	26.1	26.2

Table 6-2 Signal-to-noise ratios for probe configuration 2.

According to the tables above, the first probe configuration would be the best for measuring weak Raman signals. This was expected since there is a great loss of light in probe configuration 2 when the excitation light is guided into the measuring fiber at a skew angle. Besides the poor signal-to-noise ratio for probe configuration 2, the set-up is difficult to align properly.

The first configuration consists of six parts (lenses and filters) while the second version only consists of only four parts. Considering building the probe, it is easier to build a small probe with few parts. However, in this case, the better signal-to-noise ratio for the first configuration makes it the preferred choice.

7. Test of Probe

7.1 Introduction

The next step was to build the probe according to the chosen probe configuration in the previous chapter, see Figure 6-1. The main goal was to make the probe as small as possible and easy to align.

The probe was evaluated in the same way as in the measurements of fiber emission, i.e. by calculating the ratios between Raman peaks from Rhodamine 6G and the fiber emission background.

7.2 Final Probe Design

The probe consists of two filters, one holographic beamsplitter and, since there are three fibers connected to the probe, three positioners and three collimating lenses. The positioners and lenses used in the probe design measurements were too big and clumsy to use in a small probe. After some search, a small fiber positioner (PAF-SMA-7-NIR, Optics for Research, Inc.) with a built-in collimating lens was found and ordered. The collimating lens was anti-reflection coated for near-infrared light. The positioner allows x-y-z and ϕ-θ adjustments. The filter and beam splitter holders and the box itself were manufactured at the local workshop according to the drawings in the appendix. In Figure 7-1, a full-scale picture of the final probe with all parts included is found.

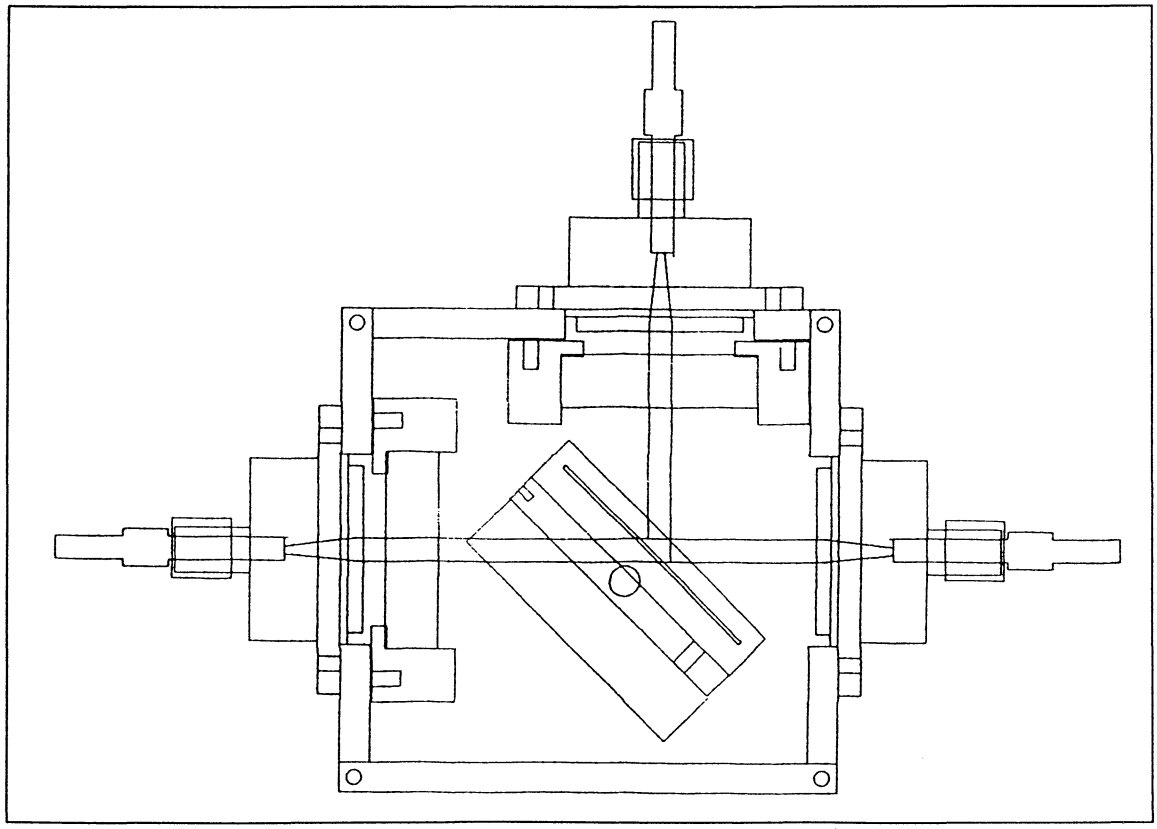

Figure 7-1 Full-scale picture of the final probe.

The dimension of the box is 66x64x56 mm. The fiber positioners could not collimate the emission from 600 μm fibers but with a small modification they were able to collimate the emission from 400 μm fibers.

7.3 Experimental Set-Up for Probe Testing

The probe was aligned and the throughputs of the fiber positioners were optimised. Two 8 meters long 400 μm Anhydroguide fibers were used for the guiding of the light to and from the probe. The probe was tested both with an 1 meter 400 μm Anhydroguide long measuring fiber and without any fiber. The fiber which guided the Raman signal to the spectrograph was connected directly to the spectrograph with a fiber coupling. The laser, spectrograph and detector were the same as in the previous measurements. The experimental set-up can be seen in Figure 7-2.

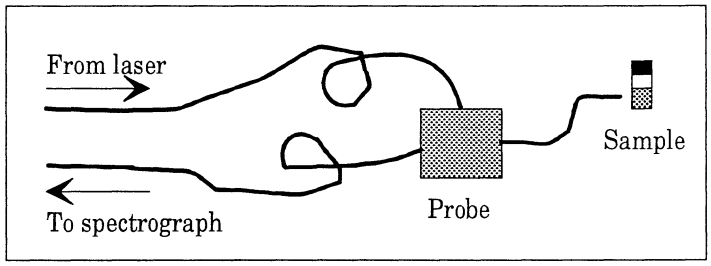

Figure 7-2 Experimental set-up for final probe testing.

The test sample was Rhodamine 6G and like in the previous measurements, the ratio between the Raman signal and the fiber emission background was calculated according to Figure 5-3.

In all measurements, the laser power was ~130mW and the output power from the measuring fiber was ~30 mW. The total acquisition time was 10 s.

7.4 Results, Discussion and Conclusion

The Raman signal from Rhodamine 6G measured with the probe with an 1 meter long measuring fiber and the pure fiber emission when the fiber was pointing out in the air is presented in Figure 7-3.

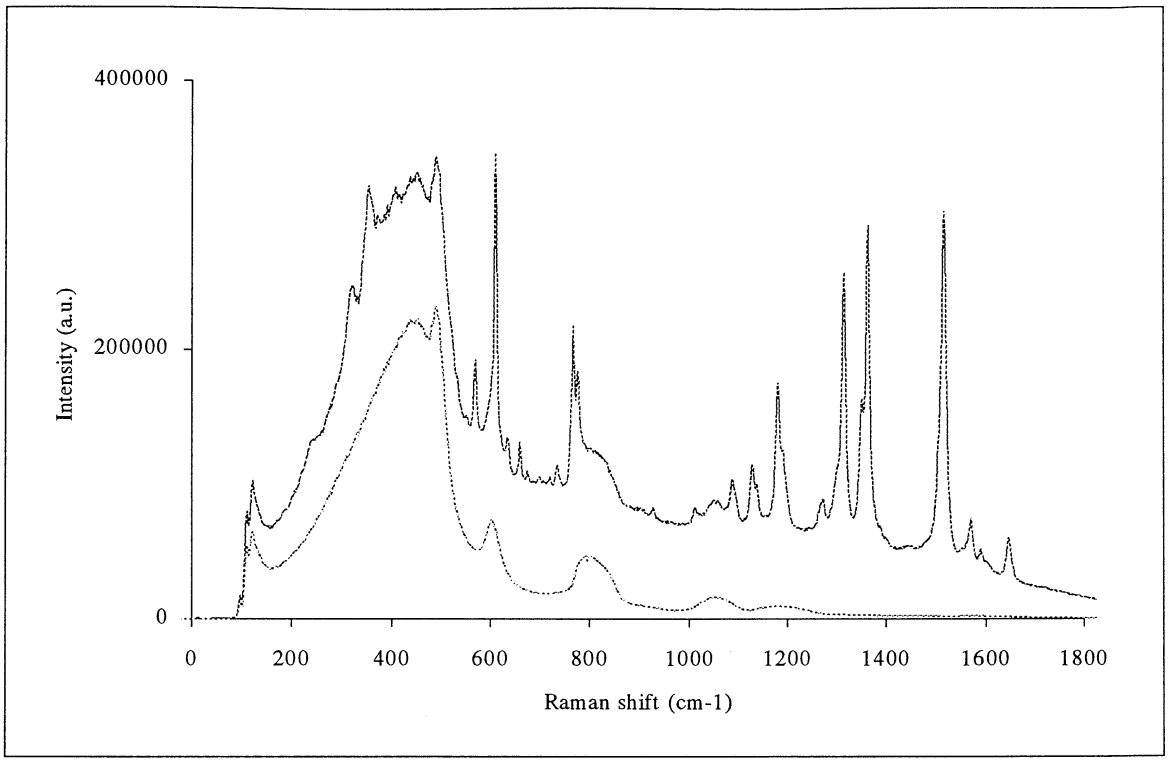

Figure 7-3 Raman signal from Rhodamine 6G+ fiber emission and pure fiber emission from the probe with 1 meter long measuring fiber.

In the figure, the Raman signals are much stronger compared to the fiber emission than in the fiber emission measurements. This was expected since the measuring fiber is 1 meter long and not 8 meters long. The ratios between the Raman signal and the fiber emission for the same peaks as in the fiber emission measurements, are tabulated in Table 7-1. The weak peak at 927 cm^{-1} has been omitted since it is very uncertain. The ratios were compared to the corresponding ratios from the fiber emission measurements of the 8 meters long 400 µm Anhydroguide fiber.

Raman shift (cm^{-1})	A Probe ratio	B Ratios from Anhydroguide 400 µm fiber emission measurements	A/B
612	2.38	0.28	8.53
661	1.35	0.16	8.23
1089	3.84	0.46	8.27
1316	61.04	9.47	6.44
1516	105.13	13.24	7.94
1646	14.57	1.61	9.07

Table 7-1 Signal improvement for Raman signal/fiber emission ratios with probe compared to an 8 meter measuring fiber.

In the right hand column, the relative increase in signal strength is on average around 8. The measuring fiber is eight times shorter than in the fiber emission measurements and thus

the signal strength increases eight times. This indicates that the effect of the probe is to allow measurements 8 meters away from the laser without introducing any new fiber emission. To further test this, the 1 meter long measuring fiber was removed and the measurement was done with the sample close to the output of the probe. In Figure 7-4, there are two curves, one with Rhodamine 6G placed close to the probe and one with an ordinary mirror in front of the probe.

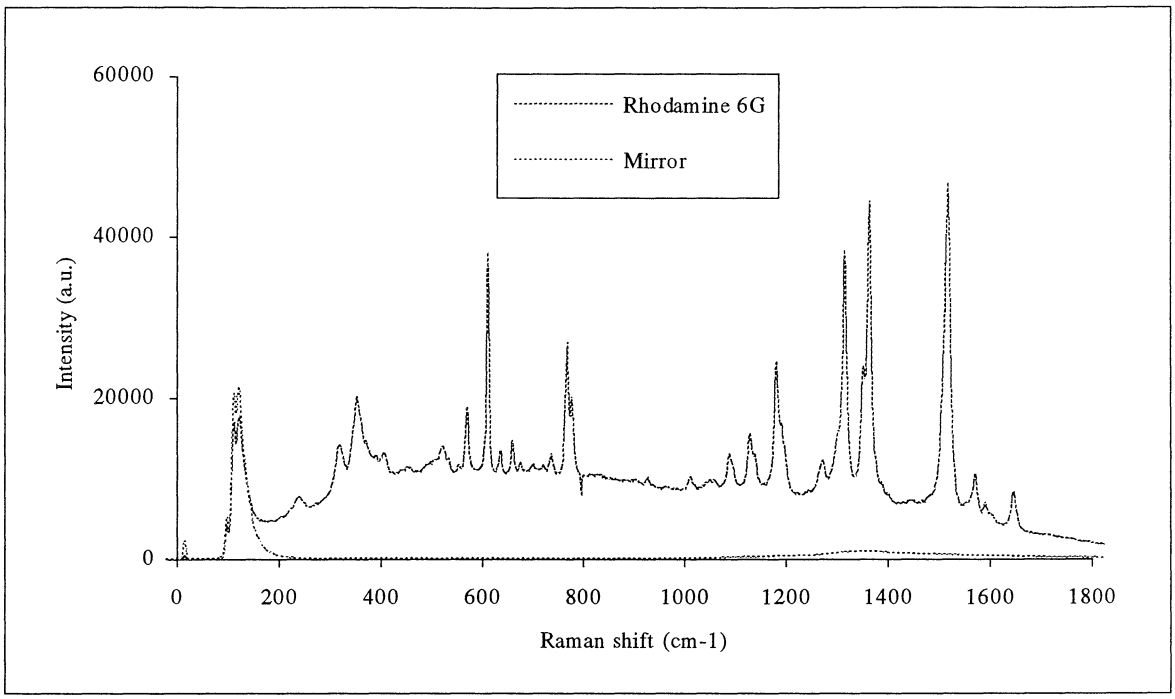

Figure 7-4 Direct probe measurements of Rhodamine 6G and measurement with a mirror in front of the probe.

The spectra from Rhodamine 6G contains a relative high fluorescence background. In order to make sure that this fluorescence really came from the Rhodamine itself and not from any component in the probe, a mirror was placed in front of the probe. The mirror reflected all outcoming light and there was no fluorescence from the probe as can be seen in the figure. The small hill at approximately 1350 cm-1 comes from light leakage at the coupling between the spectrograph and the CCD detector.

The final conclusion is that this probe makes remote measuring possible without introducing any new fiber emission. With a short fiber *in vivo* measurements can be done and it is also possible to remove the fiber and measure direct on a surface. Further, the probe is small, stable and easy to align.

8. Acknowledgements

I would like to thank my supervisor Sune Montán for his guidance, inspiration, encouragement and subtle humour.

I would also like to thank Annika Enejder who was the first person to introduce me to the work at Lund University Medical Laser Centre. After I had listen to a fascinating presentation three years ago, I knew what subject I wanted to learn more about and presumably work with after my examination.

Finally, I would like to thank Professor Sune Svanberg who always is a great source of inspiration and encouragement.

9. References

1. U. Gustafsson, "Near-Infrared Raman Spectroscopy Using a Diode Laser and CCD Detector for Tissue Diagnostics", Diploma Work, *Lund Reports on Atomic Physics*, **LRAP-138**, 1993

2. J. Bood and H. Carlsson, "Raman and Infrared Absorption Spectroscopy for Tissue Diagnostics", Diploma Work, *Lund Reports on Atomic Physics*, **LRAP-168**, 1995

3. A. Åkesson, "Near-Infrared Raman Spectroscopy for Tissue characterisation: Adaption of the Set-up for Medical use.", Diploma Work, *Lund Reports on Atomic Physics*, **LRAP-198**, 1996

4. M. Gustafsson, "Spectroscopic Studies of Tissue Using Near-Infrared Raman Microscopy", Master´s Thesis, *Lund Reports on Atomic Physics*, **LRAP-207**, 1997

5. S. Svanberg, "Atomic and Molecular Spectroscopy", *Springer Series on Atoms and Plasmas*, Volume 6, 2nd edition, 1992

6. A. Mahadevan-Jensen and R. Richards-Kortum, "Raman Spectroscopy for the Detection of Cancers and Precancers", *Journal of Biomedical Optics*, **1**(1), 31, 1996

7.B. Chase, "A New Generation of Raman Instrumentation", *Applied Spectroscopy*, **48**(7), 14A, 1994

8. M.M. Carabba, K.M. Spencer, C. Rich and D. Rauh, "The Utilization of a Holographic Bragg Diffraction Filter for Rayleigh Line Rejection in Raman Spectroscopy", *Applied Spectroscopy,* **44**(9), 1558, 1990

9. D.E. Battery, J.B. Slater, R. Wludyka, H. Owen, D.M. Pallister and M.D. Morris, "Axial Transmissive f/1.8 Imaging Raman Spectrograph with Volume-Phase Holographic Filter and Grating", *Applied Spectroscopy,* **47**(11), 1913, 1993

10. Kaiser Optical Systems, Inc., "Holospec VPT System^{TM} Operations Manual", October 17, 1994

11. Princeton Instruments, Inc., "LN/CCD Detector Operation Manual", October 28, 1994

12. A.P. Shreve, N.J. Cherepy and R.A. Mathies, "Effective Rejection of Fluorescence Interference in Raman Spectroscopy Using a Shifted Exitation Difference Technique", *Applied Spectroscopy,* **46**(4), 707, 1992

13. P.A. Mosier-Boss, S.H. Lieberman and R. Newbery, "Fluorescence Rejection in Raman Spectroscopy by Shifted-Spectra, Edge Detection and FFT Filtering Techniques", *Applied Spectroscopy,* **49**(5), 630, 1995

14. T. Tahei and H. Hamaguchi, "Picosecond Raman Spectroscopy Using a Streak Camera", *Applied Spectroscopy,* **47**(4), 391, 1993

15. M.G. Shim and B.C. Wilson, "The Effects of *ex vivo* Handling Procedures on the Near-Infrared Raman spectra of Normal Mammalian Tissues", *Photochemistry and Photobiology*, **63**(5), 662, 1996

16. S-G. Pettersson, S. Borgström and H. Hertz, "Advanced Optics", Departement of Physics, Lund Institute of Technology, 1995

17. M.L. Myrik, S.M. Angel and R. Desidero, "Comparison of some fiber optic configurations for measurements of fluorescence and Raman scattering", *Applied Optics*, **29**(9), 1333, 1990

18. I.R. Lewis and P.R. Griffiths, "Raman Spectroscopy with Fiber-Optic Sampling", *Applied Spectroscopy*, **50**(10), 12A, 1996

19. M.L. Myrik and S.M. Angel, "Elimination of Background in Fiber-Optic Raman Measurements", *Applied Spectroscopy*, **44**(4), 565, 1990

20. J.M. Bello and T. Vo-Dinh, "Surface-Enhanched Raman Scattering Fiber-Optic Sensor", *Applied Spectroscopy*, **44**(1), 63, 1990

21. C.D. Newman, G.G. Bret and R.L. McCreery, "Fiber-Optic Sampling Combined with an Imaging Spectrograph for Routine Raman Spectroscopy", *Applied Spectroscopy*, **46**(2), 262, 1992

22. N.Q. Huy, M. Jouan and N.Q. Dao, "Use of a Mono-Fiber Optrode in Remote and *in Situ* Measurements by the Raman /Laser/Fiber Optics (RLFO) Method", *Applied Spectroscoopy*, **47**(12), 2013, 1993

23. Princeton Instruments, Inc., "WinSpec User's Manual", September 4, 1996

24. D.A. Carter, W.R. Thompson, C.E. Taylor and J.E. Pemberton, "Frequency / Wavelength Calibration of Multipurpose Multichannel Raman Spectrometers. Part II: Calibration Fit Considerations and Calibration Standards", *Applied Spectroscopy*, **49**(11), 1561, 1995

10. Appendix

Below, all drawings of the box, filter and beam splitter holders are presented. All drawings are shown in full scale.

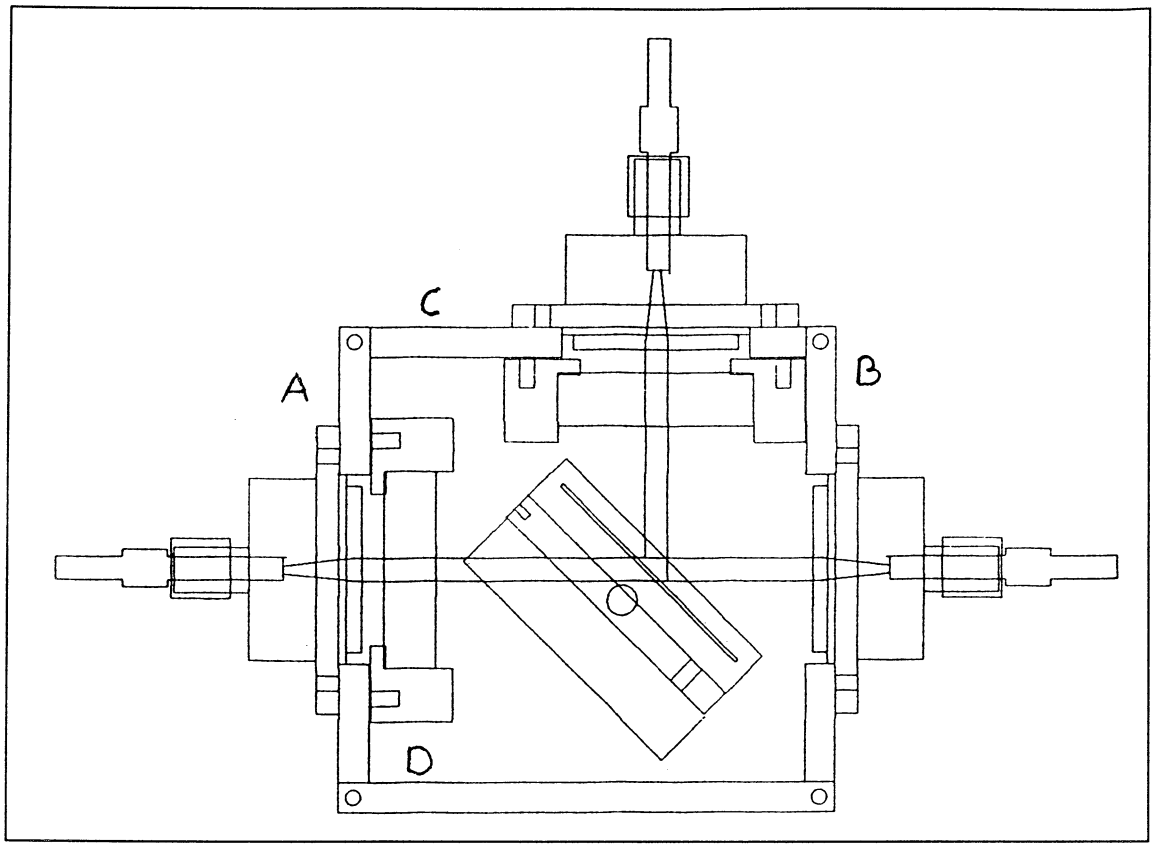

Figure 10-1 Owerview of the box with positioners, filter and beamsplitter holders.

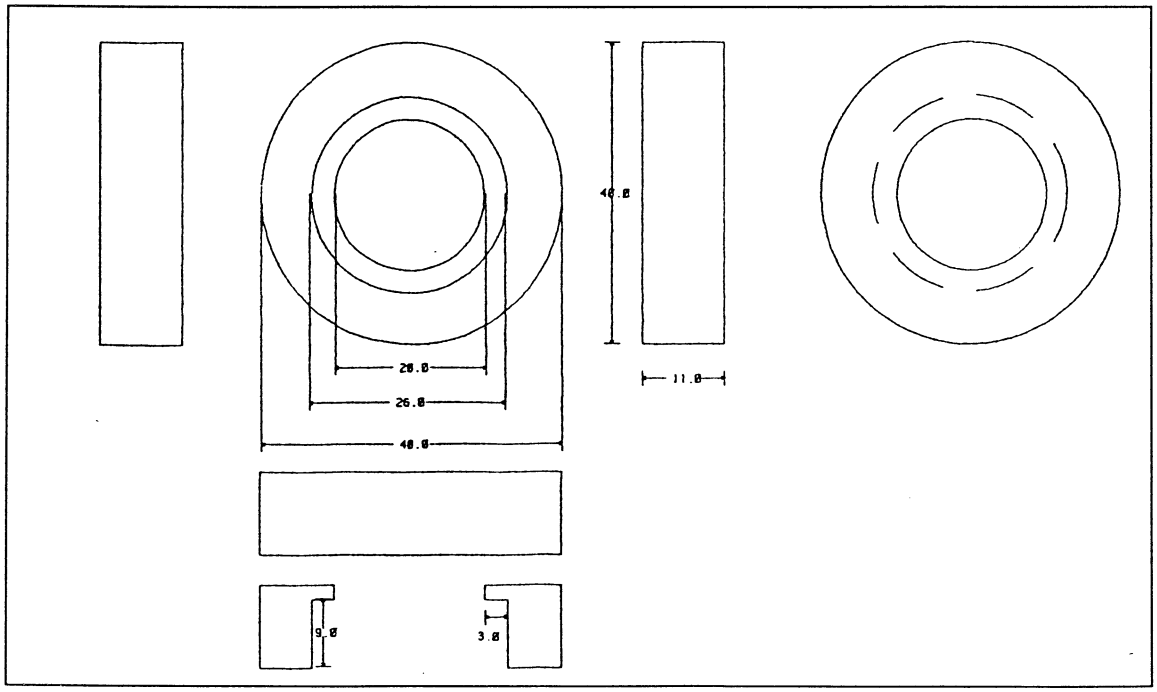

Figure 10-2 Drawing of filter holder.

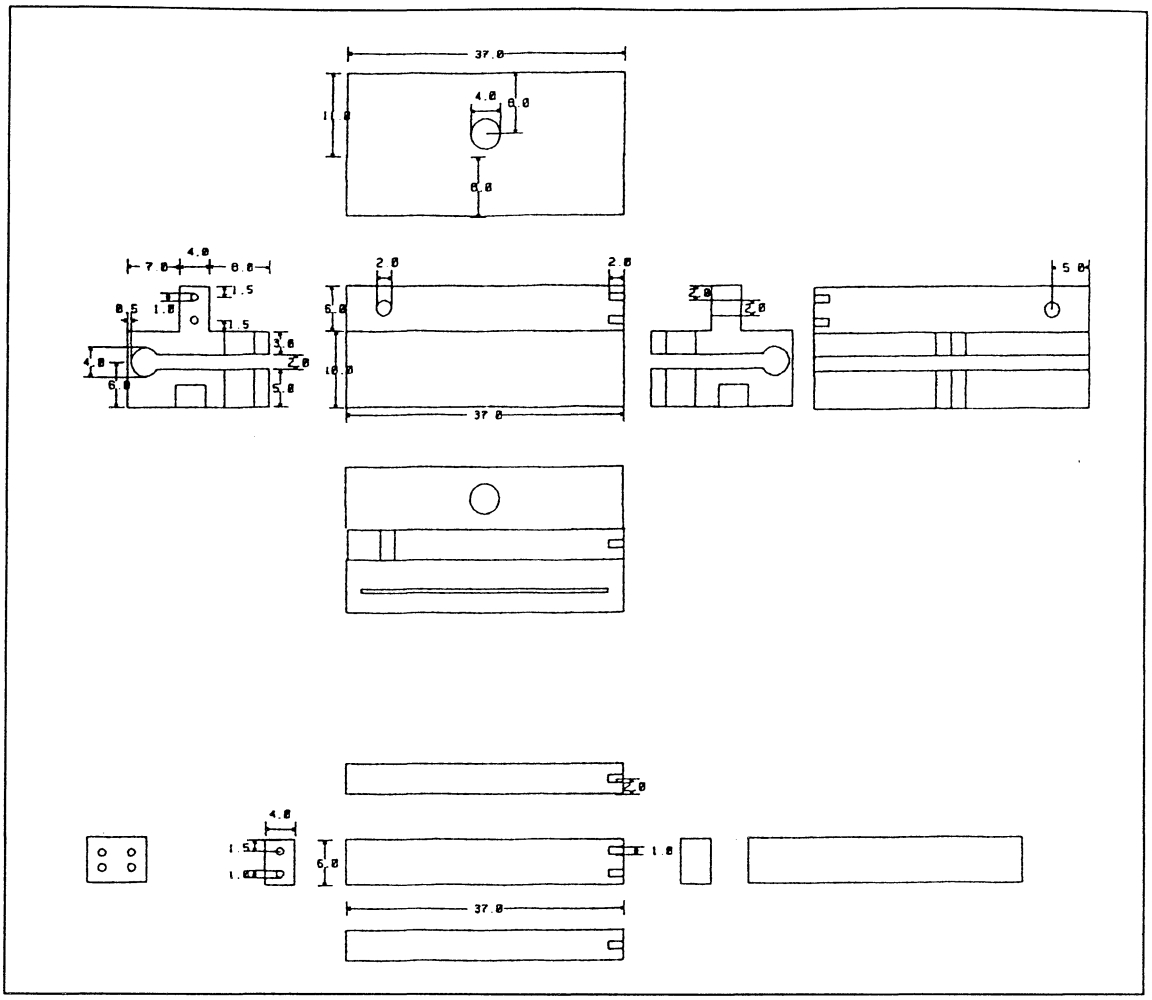

Figure 10-3 Drawing of holographic beamsplitter holder.

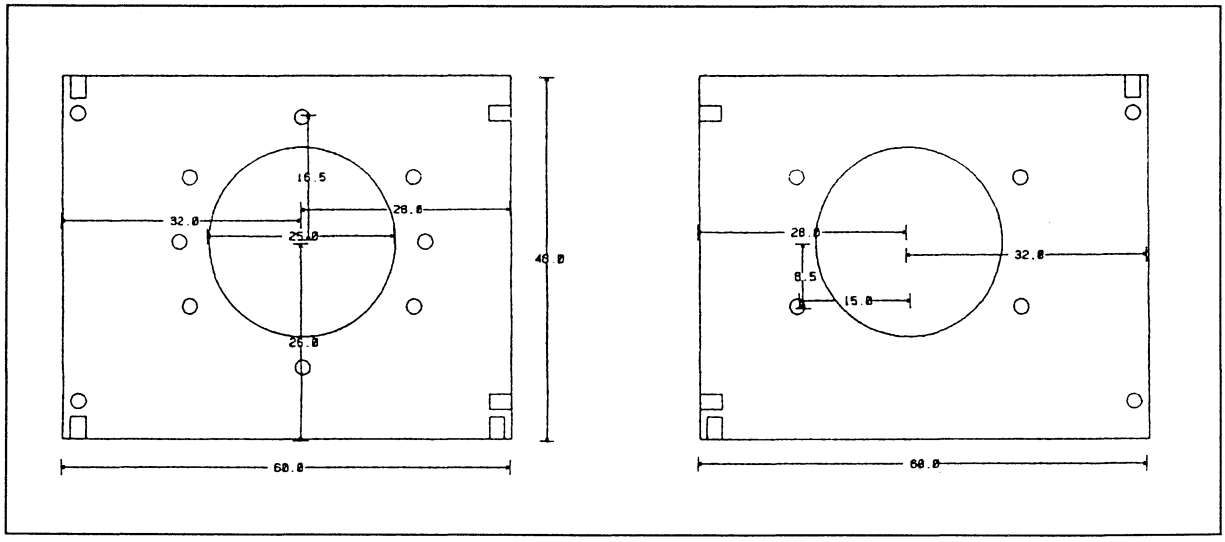

Figure 10-4 Drawing of A and B side, see Figure 10-1.

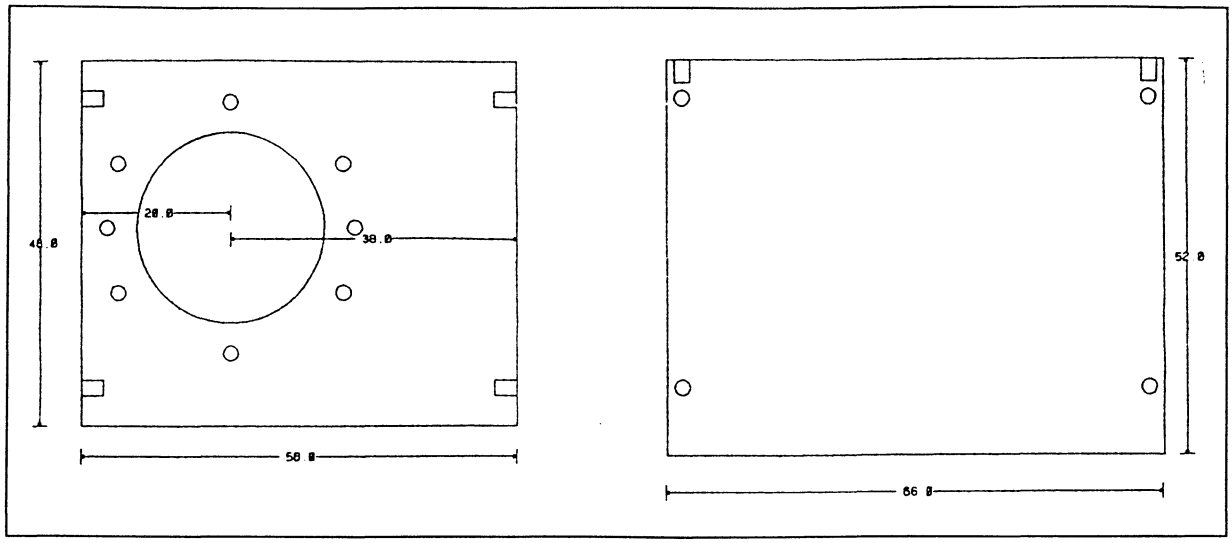

Figure 10-5 Drawing of C and D side, see Figure 10-1.

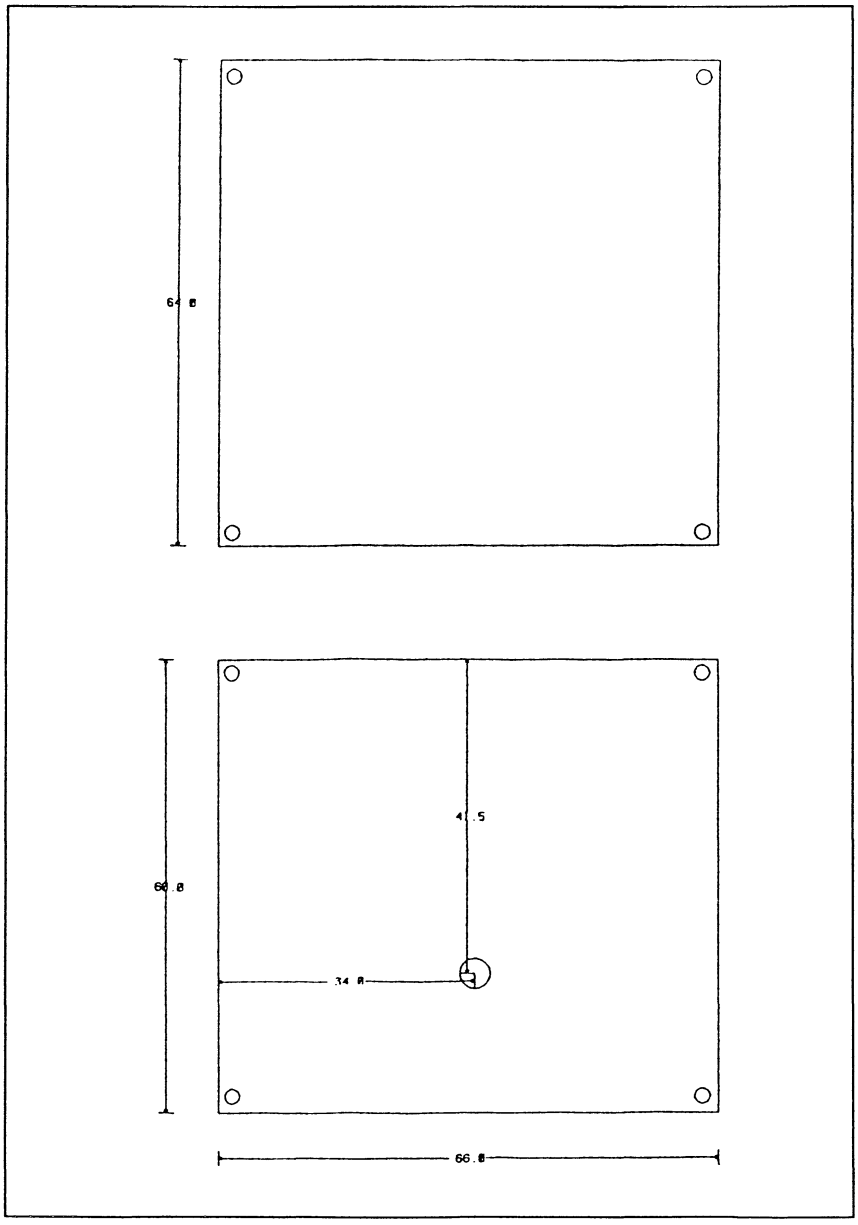

Figure 10-6 Drawing of top and bottom of the box.